Pilot Sequence Assisted Channel Estimation in MIMO/SIMO/SISO-OFDM Systems

Xiao Zhou
Shandong University
Chengyou Wang (wangchengyou@sdu.edu.cn)
School of Mechanical, Electrical and Information Engineering, Shandong University, Weihai 264209, China https://orcid.org/0000-0002-0901-2492
Qun Wu
Shandong University

Research

Keywords: Channel estimation, pilot sequence (PS), multiple input multiple output-orthogonal frequency division multiplexing (MIMO-OFDM), single input multiple output-orthogonal frequency division multiplexing (SIMO-OFDM), single input single output-OFDM (SISO-OFDM), space time block coding (STBC), bit error rate (BER)

Posted Date: October 14th, 2020

DOI: https://doi.org/10.21203/rs.3.rs-89451/v1

Pilot Sequence Assisted Channel Estimation in MIMO/SIMO/SISO-OFDM Systems

Xiao Zhou, Chengyou Wang*, Qun Wu

School of Mechanical, Electrical and Information Engineering, Shandong University, Weihai 264209, China
**Corresponding author: wangchengyou@sdu.edu.cn*

Abstract: For improving the communication system performance in multiple input multiple output-orthogonal frequency division multiplexing (MIMO-OFDM) system, single input multiple output-orthogonal frequency division multiplexing (SIMO-OFDM) system, single input single output-orthogonal frequency division multiplexing (SISO-OFDM) system, this paper introduces a pilot assisted channel estimation method. The proposed method is a combination of pilots and channel estimation based on known channel state information (CSI). First, the pilots are used to maintain the orthogonality characteristics of space time block coding (STBC). By designing the interference-free pilots we estimating the channel, and then with the pre-estimated channel characteristics data is decoded at the MIMO-OFDM system receiver. In this paper, we proposed four kinds of comb-type pilot sequences with interference-free pilots designing among consecutive subcarriers. The proposed pilot assisted channel estimation method in MIMO/SIMO/SISO-OFDM systems could be well adopted with different low and high order modulations. This flexible transmission mechanism can save pilot overhead and has strong anti-interference ability in dynamic channels. Moreover, high-order constellation modulation level will enhance the channel capacity in MIMO/SIMO/SISO-OFDM system. Therefore, it can be used as a candidate technology for 5G or 6G MIMO/SIMO/SISO-OFDM system.

Keywords: Channel estimation, pilot sequence (PS), multiple input multiple output-orthogonal frequency division multiplexing (MIMO-OFDM), single input multiple output-orthogonal frequency division multiplexing (SIMO-OFDM), single input single output-OFDM (SISO-OFDM), space time block coding (STBC), bit error rate (BER)

1. Introduction

Orthogonal frequency division multiplexing (OFDM) system is characterized by its robustness to the multipath induced inter-symbol interference (ISI) [1], [2]. Foschini *et al.* [3], [4] showed that antenna diversity can be exploited to significantly enhance spectral efficiency by using multiple antennas at both transmitter and receiver. Recently, space time block coding (STBC) has been proposed as an efficient way to achieve this capacity improvement for the multiple input multiple output (MIMO) channel. MIMO/ single input multiple output (SIMO)/single input single output (SISO)-OFDM systems are recognized as the promising technology for 5G and 6G mobile communications.

When MIMO is used with OFDM, such as STBC based transmit diversity, channel state information (CSI) [5] is required for coherent detection and decoding. CSI can be obtained in two categories. The first one is blind pilots, and the second one is based on pilots which are known beforehand at the receiver. In STBC MIMO-OFDM systems, different symbols are transmitted from different antennas simultaneously, and consequently, the received signal is the superposition of these signals. The designed pilot sequence (PS) must be orthogonal among transmit antennas [6]. Optimal pilot sequences were first proposed in [7]–[10] for MIMO-OFDM systems. Chern *et al*. [11] proposed a prime PS to one transmit antenna. The sequences of other transmit antennas are phase shift in frequency domain, or cyclic shift in time domain, to the prime sequence. Del Peral-Rosado *et al.* [12] proposed an optimal placement of the pilot subcarriers with regard to the mean square error (MSE) of the least square (LS) channel estimation for SISO-OFDM systems. Younas *et al.* [13] proposed a classical MIMO transmission with pilot aided sequences based on adaptive LS channel estimation in a correlated time varying channel. It simplifies the LS channel estimation by utilizing the proposed pilot construction to avoid matrix inversion which causes great complexity of the receiver. LMMSE and SVD channel estimation methods are widely utilized in multi-user MIMO-OFDM systems [14]–[17], but they inevitably bring a large amount of matrix calculation in frequency domain.

For virtual multiple-input single-output (MISO)-OFDM systems, Wang *et al.* [18] proposed an efficient resource allocation method to provide high transmission throughput. The base stations (BS) can allocate subcarriers to transmit node with the highest magnitude of channel frequency response (CFR) on the subcarriers. Under time varying channels, Youssefi *et al.* [19] proposed a new approach to achieve optimal training sequences (OTS) in terms of minimizing the MSE for spectrally efficient MIMO-OFDM systems. The OTS are equal powered and spaced, and orthogonal positioned.

However, in practical OFDM based systems to avoid the transmitted data, being distorted by the low pass filter, the subcarriers that fall in the roll-off region of the filter transfer function are not used, which are often referred to as virtual subcarriers [20]–[23]. The existence of virtual subcarriers breaks the equal spaced property of conventional pilot sequences and the system performance will be increased. Kenarsari-Anhari *et al.* [24] formulated the power allocation as linear programming (LP) problem in coded OFDM system. Wang *et al.* [25] proposed a low-complexity power allocation method in the cooperative OFDM networks and it can greatly improve the system throughput. The equivalent channel power gain can be calculated and the power among each subcarrier can be allocated through Lagrange optimization method. The complexity is linear in the number of subcarriers, which is attractive in practical application for OFDM networks.

In most STBC MIMO schemes, the interference between the two transmit braches degrades the performance of communication system severely. To improve communication performance and obtain diversity gains, the paper proposes a novel interlaced pilot sequence channel estimation method in STBC MIMO-OFDM systems which suppresses the ISI and inter-carrier interference (ICI) effectively. In addition, the total available bandwidth using the STBC pre-coder could provide high channel capacity in MIMO-OFDM systems.

This paper introduces an interlaced PS assisted channel estimation method in MIMO/SIMO/SISO-OFDM systems to combat the interference induced by Rayleigh fading channels. Simulation results show that the proposed channel estimation method based on interlaced PS could provide significant diversity gains in MIMO/SIMO/SISO-OFDM system under different modulation modes.

The remainder of this paper is organized as follows. The MIMO/SIMO/SISO-OFDM system models are presented in Section II. Section III introduces pilot assisted channel estimation. Section IV illustrates Rayleigh channel model. Simulation results and comparison analysis are presented in Section V. Section VI concludes the paper.

2. MIMO/SIMO/SISO-OFDM System Models

2.1 MIMO/SISO-OFDM System Model

Fig. 1 and Fig. 2 illustrate the MIMO-, and SISO-OFDM systems, respectively. In this paper, we consider the MIMO-OFDM system with the number of transmit and receive antennas $N_{\mathrm{T}}^{1}=2$, $N_{\mathrm{R}}^{1}=2$, and SISO-OFDM system with $N_{\mathrm{T}}^{2}=1$, $N_{\mathrm{R}}^{2}=1$.

At the transmitter side, the input bits are grouped and mapped according to a pre-specified constellation modulation scheme. The SISO-OFDM and MIMO-OFDM systems could adopt different kinds of modulation patterns, such as binary phase shift keying (BPSK), quadrature phase shift keying (QPSK), 8 phase shift keying (8PSK), 16 quadrature amplitude modulation (16QAM) and 64 quadrature amplitude modulation (64QAM) [26]. The higher order modulation mode, the more bits an OFDM symbol carries, the more information the MIMO-OFDM system transmits. Therefore, higher order modulation can improve the transmission efficiency of MIMO-OFDM.

2.2 MIMO-, SIMO-, SISO-OFDM System Model

After constellation modulation, the modulated symbols are sent to space-time encoder. According to Alamouti criterion, the space-time coded signals are allocated to two antennas. After STBC [2], the transmitted OFDM codeword could be expressed as:

$$\boldsymbol{X}=\begin{bmatrix}\boldsymbol{X}_i & -\boldsymbol{X}_{i+1}^{*}\\ \boldsymbol{X}_{i+1} & \boldsymbol{X}_i^{*}\end{bmatrix}. \tag{1}$$

Correspondingly, the transmit OFDM symbols on the transmit antenna one could be represented as:

$$\boldsymbol{X}^1=[\boldsymbol{X}_i \quad -\boldsymbol{X}_{i+1}^{*}]. \tag{2}$$

Similarly, the transmit OFDM symbols on the transmit antenna two could be represented as:

$$\boldsymbol{X}^2=[\boldsymbol{X}_{i+1} \quad \boldsymbol{X}_i^{*}]. \tag{3}$$

The received OFDM symbols $\boldsymbol{Y}$ are the superposition coming from transmit antenna one and two. After STBC in the transmitter, the comb-type pilots are inserted through the time domain by fixed intervals of subcarriers. Figs. 1 and 2 illustrate the system models of SISO-OFDM and MIMO-OFDM, respectively. As shown in Fig. 2, the inverse fast Fourier transform (IFFT) block is used to transform the data sequence $\boldsymbol{X}^1$ and $\boldsymbol{X}^2$ into time-domain signal $\boldsymbol{x}^1$ and $\boldsymbol{x}^2$ on the transmit antenna one, which can be shown as:

$$\boldsymbol{x}^1(n)=\frac{1}{\sqrt{N}}\sum_{k=0}^{N-1}\boldsymbol{X}^1(k)\mathrm{e}^{\mathrm{j}2\pi kn/N},\ \ 0\le n\le N-1. \tag{4}$$

$$\boldsymbol{x}^2(n)=\frac{1}{\sqrt{N}}\sum_{k=0}^{N-1}\boldsymbol{X}^2(k)\mathrm{e}^{\mathrm{j}2\pi kn/N},\ \ 0\le n\le N-1. \tag{5}$$

where $n = 0,1,2,\cdots,N-1$ is sampling points, N is the length of IFFT and $\mathrm{e}^{\mathrm{j}2\pi/N}$ is the twiddle factor of IFFT. After removing the CP, the time-domain received OFDM symbols are transformed into frequency domain in single fast Fourier transform (FFT) blocks. The received frequency-domain signals $\boldsymbol{Y}^1(k)$ and $\boldsymbol{Y}^2(k)$ on the receive antenna one and two could be represented as:

$$\boldsymbol{Y}^1(k) = \boldsymbol{X}^1(k)\boldsymbol{H}^1(k) + \boldsymbol{W}^1(k), \quad 0 \le n \le N-1. \tag{6}$$

$$\boldsymbol{Y}^2(k) = \boldsymbol{X}^2(k)\boldsymbol{H}^2(k) + \boldsymbol{W}^2(k), \quad 0 \le n \le N-1. \tag{7}$$

where $\boldsymbol{W}^1(k)$ and $\boldsymbol{W}^2(k)$ are the frequency-domain AWGN.

After removing the CP, the time-domain received OFDM symbols are transformed into frequency domain in two FFT blocks in the MIMO-OFDM systems. The received frequency-domain signals could be represented as:

$$\boldsymbol{Y}^1(k) = \frac{1}{\sqrt{N}}\sum_{n=0}^{N-1}\boldsymbol{y}^1(n)\mathrm{e}^{-\mathrm{j}2\pi kn/N}, \quad 0 \le k \le N-1. \tag{8}$$

$$\boldsymbol{Y}^2(k) = \frac{1}{\sqrt{N}}\sum_{n=0}^{N-1}\boldsymbol{y}^2(n)\mathrm{e}^{-\mathrm{j}2\pi kn/N}, \quad 0 \le k \le N-1. \tag{9}$$

where $k = 0,1,2,\cdots,N-1$ represents the index of subcarriers and $\mathrm{e}^{-\mathrm{j}2\pi/N}$ is the twiddle factor of FFT. where $\boldsymbol{y}^1$ and $\boldsymbol{y}^2$ are the time-domain received OFDM complex value symbols after multipath fading and AWGN from receive antenna one and receive antenna two, respectively. $\boldsymbol{Y}^1$ and $\boldsymbol{Y}^2$ are the frequency domain received OFDM complex value symbols after multipath fading and AWGN from receive antenna one and receive antenna two, respectively.

In the receiver of MIMO-OFDM system, the frequency-domain symbols are decoded in the space-time block decoding (STBD). The signals at multiple receive antennas are decoded using CSI provided by the channel equalizer. Therefore, channel equalizer is a critical module of MIMO-OFDM systems supposing that the CSI is known to the MIMO-OFDM receiver. At last, the binary information bits are obtained after the BPSK, QPSK, 8PSK, 16QAM [26], and 64QAM constellation demodulation.

2.3 STBD IN MIMO-OFDM System Model

Diversity gains can be obtained by using STBC technology at the transmitter. In MIMO-OFDM systems, STBC is a key technology to improve the system performance. STBC technology is used to encode signals in the frequency domain. Alamouti code is a complex orthogonal STBC specially designed for two transmit antennas [1], [2].

According to the estimated CFR, the OFDM symbol after STBD in the receiver can be shown as:

$$\begin{bmatrix} \hat{\boldsymbol{X}}_1 \\ \hat{\boldsymbol{X}}_2 \end{bmatrix} = \begin{bmatrix} \dfrac{\hat{\boldsymbol{Y}}_{11}\hat{\boldsymbol{H}}_{11}^* + \hat{\boldsymbol{Y}}_{12}^*\hat{\boldsymbol{H}}_{21} + \hat{\boldsymbol{Y}}_{21}\hat{\boldsymbol{H}}_{12}^* + \hat{\boldsymbol{Y}}_{22}^*\hat{\boldsymbol{H}}_{22}}{\hat{\boldsymbol{H}}_{11}\hat{\boldsymbol{H}}_{11}^* + \hat{\boldsymbol{H}}_{21}\hat{\boldsymbol{H}}_{21}^* + \hat{\boldsymbol{H}}_{12}\hat{\boldsymbol{H}}_{12}^* + \hat{\boldsymbol{H}}_{22}\hat{\boldsymbol{H}}_{22}^*} \\ \dfrac{\hat{\boldsymbol{Y}}_{11}\hat{\boldsymbol{H}}_{21}^* - \hat{\boldsymbol{Y}}_{12}^*\hat{\boldsymbol{H}}_{11} + \hat{\boldsymbol{Y}}_{21}\hat{\boldsymbol{H}}_{22}^* - \hat{\boldsymbol{Y}}_{22}^*\hat{\boldsymbol{H}}_{12}}{\hat{\boldsymbol{H}}_{11}\hat{\boldsymbol{H}}_{11}^* + \hat{\boldsymbol{H}}_{21}\hat{\boldsymbol{H}}_{21}^* + \hat{\boldsymbol{H}}_{12}\hat{\boldsymbol{H}}_{12}^* + \hat{\boldsymbol{H}}_{22}\hat{\boldsymbol{H}}_{22}^*} \end{bmatrix}. \tag{10}$$

where $\hat{\boldsymbol{X}}_1$ and $\hat{\boldsymbol{X}}_2$ are the 1st and 2nd STBD OFDM symbols, respectively. In MIMO-OFDM system, $\hat{\boldsymbol{Y}}_{11}$, $\hat{\boldsymbol{Y}}_{12}$, $\hat{\boldsymbol{Y}}_{21}$, and $\hat{\boldsymbol{Y}}_{22}$ are the received symbols transmitted from transmit antenna one to receive antenna one, from transmit antenna one to receive antenna two, from transmit antenna two to receive antenna one, from transmit antenna two to receive antenna two, which could be represented as:

$$\begin{cases} \hat{\boldsymbol{Y}}_{11} = \boldsymbol{Y}_{11} + \hat{\boldsymbol{W}}_{11}, \\ \hat{\boldsymbol{Y}}_{12} = \boldsymbol{Y}_{12} + \hat{\boldsymbol{W}}_{12}, \\ \hat{\boldsymbol{Y}}_{21} = \boldsymbol{Y}_{21} + \hat{\boldsymbol{W}}_{21}, \\ \hat{\boldsymbol{Y}}_{22} = \boldsymbol{Y}_{22} + \hat{\boldsymbol{W}}_{22}. \end{cases} \tag{11}$$

where $\hat{\boldsymbol{W}}_{11}$, $\hat{\boldsymbol{W}}_{12}$, $\hat{\boldsymbol{W}}_{21}$ and $\hat{\boldsymbol{W}}_{22}$ are the frequency domain AWGN between transmit antenna one to receive antenna one, transmit antenna one to receive antenna two, transmit antenna two to receive antenna one, transmit antenna two to receive antenna two, respectively. $\boldsymbol{H}_{11}$, $\boldsymbol{H}_{12}$, $\boldsymbol{H}_{21}$, and $\boldsymbol{H}_{22}$ represent the estimated CFR between transmit antenna one to receive antenna one, transmit antenna one to receive antenna two, transmit antenna two to receive antenna one, transmit antenna two to receive antenna two, respectively.

For simplicity, the Eq. (10) could be represented as:

$$\begin{bmatrix} \hat{\boldsymbol{X}}_1 \\ \hat{\boldsymbol{X}}_2 \end{bmatrix} = \begin{bmatrix} \dfrac{\hat{\boldsymbol{Y}}_{11}\hat{\boldsymbol{H}}_{11}^{*} + \hat{\boldsymbol{Y}}_{12}^{*}\hat{\boldsymbol{H}}_{21} + \hat{\boldsymbol{Y}}_{21}\hat{\boldsymbol{H}}_{12}^{*} + \hat{\boldsymbol{Y}}_{22}^{*}\hat{\boldsymbol{H}}_{22}}{|\hat{\boldsymbol{H}}_{11}|^2 + |\hat{\boldsymbol{H}}_{21}|^2 + |\hat{\boldsymbol{H}}_{12}|^2 + |\hat{\boldsymbol{H}}_{22}|^2} \\ \dfrac{\hat{\boldsymbol{Y}}_{11}\hat{\boldsymbol{H}}_{21}^{*} - \hat{\boldsymbol{Y}}_{12}^{*}\hat{\boldsymbol{H}}_{11} + \hat{\boldsymbol{Y}}_{21}\hat{\boldsymbol{H}}_{22}^{*} - \hat{\boldsymbol{Y}}_{22}^{*}\hat{\boldsymbol{H}}_{12}}{|\hat{\boldsymbol{H}}_{11}|^2 + |\hat{\boldsymbol{H}}_{21}|^2 + |\hat{\boldsymbol{H}}_{12}|^2 + |\hat{\boldsymbol{H}}_{22}|^2} \end{bmatrix}. \tag{12}$$

3. Pilot Assisted Channel Estimation

In the MIMO-OFDM, SIMO-OFDM and 1×2, 1×3, 1×4, 1×10, 1×20, 1×50, 1×100, 1×200, and 1×500 SISO-OFDM systems, the number of used subcarriers, data subcarriers, pilot subcarriers, and virtual subcarriers are 1001, 990, 11, and 1047, respectively. Correspondingly, the number of data subcarriers are 500, 750, 875, 950, 980, and 990, respectively. The number of pilot subcarriers are 501, 251, 126, 51, 21, and 11, respectively. To avoid the distortion of the low-pass filter at the transmitter, the subcarriers falling in the roll-off region of the transmitter filter are generally not used to transmit data or pilots, this part of subcarriers are defined as virtual subcarriers and the length of virtual subcarriers is 1047 in MIMO/SIMO/SISO-OFDM systems.

The interference caused by Rayleigh fading channel and AWGN could exist in the four quadrants in the complex plane. The pilots in the adjacent subcarriers should be set in different quadrants to avoid interference. In this paper, four kinds of PS are chosen to be utilized in the simulation. Under the pilot interval $n=2$, $\boldsymbol{X}_{\mathrm{p},1}^{1}(k), \boldsymbol{X}_{\mathrm{p},2}^{1}(k), \boldsymbol{X}_{\mathrm{p},3}^{1}(k), \boldsymbol{X}_{\mathrm{p},4}^{1}(k)$ could be represented as:

$$\boldsymbol{X}_{\mathrm{p},1}^{1}(k) = \begin{cases} -1.5166 \\ \vdots \\ 1.5166 \\ \vdots \\ 1.5166 \\ \vdots \\ -1.5166 \\ \vdots \\ -1.5166 \end{cases}, \quad \boldsymbol{X}_{\mathrm{p},2}^{1}(k) = \begin{cases} 1.5166 \\ \vdots \\ -1.5166 \\ \vdots \\ -1.5166, \ k=[525,527,529,\cdots,1525]. \\ \vdots \\ 1.5166 \\ \vdots \\ 1.5166 \end{cases} \tag{13}$$

$$\boldsymbol{X}_{\mathrm{p},3}^{1}(k) = \begin{cases} -1.5166 \\ \vdots \\ 1.5166 \\ \vdots \\ -1.5166 \\ \vdots \\ 1.5166 \\ \vdots \\ -1.5166 \end{cases}, \quad \boldsymbol{X}_{\mathrm{p},4}^{1}(k) = \begin{cases} 1.5166 \\ \vdots \\ -1.5166 \\ \vdots \\ 1.5166, \ k=[525,527,529,\cdots,1525]. \\ \vdots \\ -1.5166 \\ \vdots \\ 1.5166 \end{cases} \tag{14}$$

Under $n=4$, $\boldsymbol{X}_{\mathrm{p},1}^{2}(k), \boldsymbol{X}_{\mathrm{p},2}^{2}(k), \boldsymbol{X}_{\mathrm{p},3}^{2}(k), \boldsymbol{X}_{\mathrm{p},4}^{2}(k)$ could be represented as:

$$\boldsymbol{X}_{\mathrm{p},1}^{2}(k) = \begin{cases} -1.5166 \\ \vdots \\ 1.5166 \\ \vdots \\ 1.5166 \\ \vdots \\ -1.5166 \\ \vdots \\ 1.5166 \end{cases}, \quad \boldsymbol{X}_{\mathrm{p},2}^{2}(k) = \begin{cases} 1.5166 \\ \vdots \\ -1.5166 \\ \vdots \\ -1.5166, \ k=[525,529,533,\cdots,1525]. \\ \vdots \\ 1.5166 \\ \vdots \\ -1.5166 \end{cases} \tag{15}$$

$$\boldsymbol{X}_{\mathrm{p},3}^{2}(k)=\begin{cases}-1.5166\\ \vdots\\ 1.5166\\ \vdots\\ -1.5166,\\ \vdots\\ 1.5166\\ \vdots\\ -1.5166\end{cases} \boldsymbol{X}_{\mathrm{p},4}^{2}(k)=\begin{cases}1.5166\\ \vdots\\ -1.5166\\ \vdots\\ 1.5166\\ \vdots\\ -1.5166\\ \vdots\\ 1.5166\end{cases},k=[525,529,533,\cdots,1525]. \tag{16}$$

Under $n=8$, $\boldsymbol{X}_{\mathrm{p},1}^{3}(k), \boldsymbol{X}_{\mathrm{p},2}^{3}(k), \boldsymbol{X}_{\mathrm{p},3}^{3}(k), \boldsymbol{X}_{\mathrm{p},4}^{3}(k)$ could be represented as:

$$\boldsymbol{X}_{\mathrm{p},1}^{3}(k)=\begin{cases}-1.5166\\ \vdots\\ 1.5166\\ \vdots\\ 1.5166\\ \vdots\\ -1.5166\\ \vdots\\ 1.5166\end{cases}, \boldsymbol{X}_{\mathrm{p},2}^{3}(k)=\begin{cases}1.5166\\ \vdots\\ -1.5166\\ \vdots\\ -1.5166,\\ \vdots\\ 1.5166\\ \vdots\\ -1.5166\end{cases} k=[525,533,541,\cdots,1525]. \tag{17}$$

$$\boldsymbol{X}_{\mathrm{p},3}^{3}(k)=\begin{cases}-1.5166\\ \vdots\\ 1.5166\\ \vdots\\ -1.5166,\\ \vdots\\ 1.5166\\ \vdots\\ 1.5166\end{cases} \boldsymbol{X}_{\mathrm{p},4}^{3}(k)=\begin{cases}1.5166\\ \vdots\\ -1.5166\\ \vdots\\ 1.5166\\ \vdots\\ -1.5166\\ \vdots\\ -1.5166\end{cases}, k=[525,533,541,\cdots,1525]. \tag{18}$$

Under $n=20$, $\boldsymbol{X}_{\mathrm{p},1}^{4}(k), \boldsymbol{X}_{\mathrm{p},2}^{4}(k), \boldsymbol{X}_{\mathrm{p},3}^{4}(k), \boldsymbol{X}_{\mathrm{p},4}^{4}(k)$ could be represented as:

$$\boldsymbol{X}_{\mathrm{p},1}^{4}(k)=\begin{cases}-1.5166\\ \vdots\\ 1.5166\\ \vdots\\ 1.5166\\ \vdots\\ -1.5166\\ \vdots\\ 1.5166\end{cases}, \boldsymbol{X}_{\mathrm{p},2}^{4}(k)=\begin{cases}1.5166\\ \vdots\\ -1.5166\\ \vdots\\ -1.5166,\\ \vdots\\ 1.5166\\ \vdots\\ -1.5166\end{cases} k=[525,545,565,\cdots,1525]. \tag{19}$$

$$\boldsymbol{X}_{\mathrm{p},3}^{4}(k)=\begin{cases}-1.5166\\ \vdots\\ 1.5166\\ \vdots\\ -1.5166,\\ \vdots\\ 1.5166\\ \vdots\\ -1.5166\end{cases} \boldsymbol{X}_{\mathrm{p},4}^{4}(k)=\begin{cases}1.5166\\ \vdots\\ -1.5166\\ \vdots\\ 1.5166\\ \vdots\\ -1.5166\\ \vdots\\ 1.5166\end{cases}, k=[525,545,565,\cdots,1525]. \tag{20}$$

Under $n=50$, $\boldsymbol{X}_{\mathrm{p},1}^{5}(k), \boldsymbol{X}_{\mathrm{p},2}^{5}(k), \boldsymbol{X}_{\mathrm{p},3}^{5}(k), \boldsymbol{X}_{\mathrm{p},4}^{5}(k)$ could be represented as:

$$\boldsymbol{X}_{\mathrm{p},1}^{5}(k)=\begin{cases}-1.5166\\ \vdots\\ 1.5166\\ \vdots\\ 1.5166\\ \vdots\\ -1.5166\\ \vdots\\ -1.5166\end{cases},\quad \boldsymbol{X}_{\mathrm{p},2}^{5}(k)=\begin{cases}1.5166\\ \vdots\\ -1.5166\\ \vdots\\ -1.5166\\ \vdots\\ 1.5166\\ \vdots\\ 1.5166\end{cases},\ k=[525,575,625,\ldots,1525]. \tag{21}$$

$$\boldsymbol{X}_{\mathrm{p},3}^{5}(k)=\begin{cases}-1.5166\\ \vdots\\ 1.5166\\ \vdots\\ -1.5166\\ \vdots\\ 1.5166\\ \vdots\\ -1.5166\end{cases},\quad \boldsymbol{X}_{\mathrm{p},4}^{5}(k)=\begin{cases}1.5166\\ \vdots\\ -1.5166\\ \vdots\\ 1.5166\\ \vdots\\ -1.5166\\ \vdots\\ 1.5166\end{cases},\ k=[525,575,625,\ldots,1525]. \tag{22}$$

Under $n=100$, $\boldsymbol{X}_{\mathrm{p},1}^{6}(k)$, $\boldsymbol{X}_{\mathrm{p},2}^{6}(k)$, $\boldsymbol{X}_{\mathrm{p},3}^{6}(k)$, $\boldsymbol{X}_{\mathrm{p},4}^{6}(k)$ could be represented as:

$$\boldsymbol{X}_{\mathrm{p},1}^{6}(k)=\begin{cases}-1.5166\\ \vdots\\ 1.5166\\ \vdots\\ 1.5166\\ \vdots\\ -1.5166\\ \vdots\\ 1.5166\end{cases},\quad \boldsymbol{X}_{\mathrm{p},2}^{6}(k)=\begin{cases}1.5166\\ \vdots\\ -1.5166\\ \vdots\\ -1.5166\\ \vdots\\ 1.5166\\ \vdots\\ -1.5166\end{cases},\ k=[525,625,725,\ldots,1525]. \tag{23}$$

$$\boldsymbol{X}_{\mathrm{p},3}^{6}(k)=\begin{cases}-1.5166\\ \vdots\\ 1.5166\\ \vdots\\ -1.5166\\ \vdots\\ 1.5166\\ \vdots\\ -1.5166\end{cases},\quad \boldsymbol{X}_{\mathrm{p},4}^{6}(k)=\begin{cases}1.5166\\ \vdots\\ -1.5166\\ \vdots\\ 1.5166\\ \vdots\\ -1.5166\\ \vdots\\ 1.5166\end{cases},\ k=[525,625,725,\ldots,1525]. \tag{24}$$

The number of pilot subcarriers for $n=2$, $n=4$, $n=8$, $n=20$, $n=50$, and $n=100$ are 501, 251, 126, 51, 21, and 11, respectively. The number of data subcarriers for $n=2$, $n=4$, $n=8$, $n=20$, $n=50$, and $n=100$ is 1001. Because the number of pilots inserted into the system is limited, so it would not waste too much frequency resources. The proposed pilot assisted channel estimation method could save valuable bandwidth in the MIMO/SIMO/SISO-OFDM systems. The interference caused by Rayleigh fading channel and AWGN could exist in the four quadrants in the complex plane [10]. The pilots in the adjacent subcarriers should be set in different quadrants to avoid interference caused by large-scale propagation and small-scale propagation. The coherent time in Rayleigh fading channel [27] of the MIMO-OFDM system could be represented as:

$$T_{\mathrm{c}}=\frac{9}{16\pi f_{\mathrm{d}}^{2}}. \tag{25}$$

where f_{d} is the Doppler spread and can be represented as [28]:

$$f_{\mathrm{d}}=\frac{\upsilon}{\lambda}. \tag{26}$$

where υ is the mobile speed and λ is the wavelength. Under the condition of $f_{\mathrm{d}} = 20\,\mathrm{Hz}$, according to (16), the coherent time $T_{\mathrm{c}} = 4.4762\times10^{-4}\,\mathrm{s}$. Under the condition of $f_{\mathrm{d}} = 60\,\mathrm{Hz}$, the coherent time $T_{\mathrm{c}} = 4.9736\times10^{-5}\,\mathrm{s}$. Under the condition of $f_{\mathrm{d}} = 80\,\mathrm{Hz}$, the coherent time $T_{\mathrm{c}} = 2.7976\times10^{-5}\,\mathrm{s}$. When the Doppler spread f_{d} becomes large, the coherent time T_{c} becomes short, the multipath channel undergoes deep time selective fading. The smaller value the coherence time T_{c}, the more serious the complex transmitted signal decays.

Fig. 3 illustrates large-scale propagation and small-scale propagation of the STBC MIMO-OFDM. When f_{d} increases, it would induce time selective propagation, which is illustrated in Fig. 3. The time selective propagation includes large-scale propagation and small-scale propagation. To suppress the interference which is caused by small-scale propagation, the pilots are inserted in comb-type manner through the subcarriers in the frequency domain with different pilot intervals.

Fig. 4 illustrates SIMO-OFDM models utilized in micro-cell and macro-cell. According to the number of receive antennas, 1×2 SIMO-OFDM, 1×3 SIMO-OFDM, 1×4 SIMO-OFDM could be utilized in micro-cell and 1×5 SIMO-OFDM, 1×500 SIMO-OFDM could be utilized in macro-cell. The base station (BS) in the micro-cell/macro-cell could adjust the transmission power according to either the different modulation mode, such as BPSK, QPSK, 8PSK, 16QAM, 64QAM, or the transmission distance from BS to mobile station (MS). Fig. 4(a), (b), and (c) belong to micro-cell OFDM systems. As shown in Fig. 4(a), MS1 and MS2 could receive OFDM symbols from two antennas. As shown in Fig. 4(b), MS1, MS2, and MS3 could receive OFDM symbols from three antennas. As illustrated in Fig. 4(c), MS1, MS2, MS3, and MS4 could receive OFDM symbols from four antennas independently. Fig. 4(d), (e), (f), (g), (h), and (i) belong to macro-cell OFDM symbols. As illustrated in Fig. 4(d), ten antennas could receive OFDM symbols irrelevantly. It could be seen from Fig. 4(e), (f), (g), (h), and (i) that twenty, fifty, one hundred, two hundred, five hundred antennas could receive OFDM symbols irrelevantly.

4. Rayleigh Channel Model

The multipath fading channels obey Rayleigh distribution and the power distribution function (PDF) of transmit signals $\boldsymbol{x}_1$ and $\boldsymbol{x}_2$ obeys Rayleigh distribution, which could be represented as [29], [30]:

$$f_{\mathrm{Ra}}(\boldsymbol{x}_1) = \frac{\boldsymbol{x}_1}{\hat{\sigma}^2_{\alpha,\beta}} \mathrm{e}^{-\frac{\boldsymbol{x}_1^2}{2\hat{\sigma}^2_{\alpha,\beta}}}, \quad \boldsymbol{x}_1 > 0. \tag{27}$$

$$f_{\mathrm{Ra}}(\boldsymbol{x}_2) = \frac{\boldsymbol{x}_2}{\hat{\sigma}^2_{\alpha,\beta}} \mathrm{e}^{-\frac{\boldsymbol{x}_2^2}{2\hat{\sigma}^2_{\alpha,\beta}}}, \quad \boldsymbol{x}_2 > 0. \tag{28}$$

where $\hat{\sigma}_{\alpha,\beta}$ denotes the noise standard deviation from the transmit antenna α to receive antenna β. In the multipath fading environments, if there are light of sight (LOS) signals from transmit antenna to receive antenna, the transmit signals $\boldsymbol{x}_1$, $\boldsymbol{x}_2$ could obey Rice distribution, which is

$$f_{\mathrm{Ri}}(\boldsymbol{x}_1) = \frac{\boldsymbol{x}_1}{\hat{\sigma}^2_{\alpha,\beta}} \mathrm{e}^{-\frac{\boldsymbol{x}_1^2 + \mathrm{A}^2}{2\hat{\sigma}^2_{\alpha,\beta}}} \cdot \mathrm{I}_0\left(\frac{\boldsymbol{x}_1 A}{\hat{\sigma}^2_{\alpha,\beta}}\right), \quad \boldsymbol{x}_1 > 0. \tag{29}$$

$$f_{\mathrm{Ri}}(\boldsymbol{x}_2) = \frac{\boldsymbol{x}_2}{\hat{\sigma}^2_{\alpha,\beta}} \mathrm{e}^{-\frac{\boldsymbol{x}_2^2 + \mathrm{A}^2}{2\hat{\sigma}^2_{\alpha,\beta}}} \cdot \mathrm{I}_0\left(\frac{\boldsymbol{x}_2 A}{\hat{\sigma}^2_{\alpha,\beta}}\right), \quad \boldsymbol{x}_2 > 0. \tag{30}$$

where A is the peak value of the main signal amplitude and $I_0(\cdot)$ is the modified Bessel function of order zero with type one. When $A \to 0$, $f_{\mathrm{Ri}}(\boldsymbol{x}_1)$ and $f_{\mathrm{Ri}}(\boldsymbol{x}_2)$ would tend to $f_{\mathrm{Ra}}(\boldsymbol{x}_1)$ and $f_{\mathrm{Ra}}(\boldsymbol{x}_2)$.

Under Rayleigh distribution, the PDF of the complex transmitted symbols $f_{\mathrm{Ra}}(\boldsymbol{x})$ could be represented as:

$$f_{\mathrm{Ra}}(\boldsymbol{x}) = f_{\mathrm{Ra}}(\boldsymbol{x}_1)\cdot f_{\mathrm{Ra}}(\boldsymbol{x}_2), \quad \boldsymbol{x}_1 > 0, \boldsymbol{x}_2 > 0. \tag{31}$$

Under Rice distribution, the PDF of the complex transmitted symbols $f_{\mathrm{Ri}}(\boldsymbol{x})$ could be represented as:

$$f_{\mathrm{Ri}}(\boldsymbol{x}) = f_{\mathrm{Ri}}(\boldsymbol{x}_1)\cdot f_{\mathrm{Ri}}(\boldsymbol{x}_2), \quad \boldsymbol{x}_1 > 0, \boldsymbol{x}_2 > 0. \tag{32}$$

Fig. 5 illustrates the Rayleigh distribution under different noise standard deviation. $\hat{\sigma}^{1,1}_{\alpha,\beta}$, $\hat{\sigma}^{1,2}_{\alpha,\beta}$, $\hat{\sigma}^{2,1}_{\alpha,\beta}$ and $\hat{\sigma}^{2,2}_{\alpha,\beta}$ denote the noise standard deviation from transmit antenna one to receive antenna one, transmit antenna one to receive antenna two, transmit antenna two to receive antenna one and transmit antenna two to receive antenna two, respectively. It could be seen from Fig. 5 that, if $\boldsymbol{x} \ge 1.4$, $f(\boldsymbol{x})$ becomes very low. In the MATLAB simulation, $\hat{\sigma}_{\alpha,\beta} \approx 0.59$, thus $2.37\hat{\sigma}_{\alpha,\beta} \approx 1.4$. It could be seen from Fig. 4 that when $\boldsymbol{x} \ge 2.37\hat{\sigma}_{\alpha,\beta}$, the value of $f(\boldsymbol{x})$ is small. Therefore, the value of pilots should be set in the interval of $[1.4, 1.6]$.

5. Simulation Results and Comparison Analysis

This section presents the bit error rate (BER) performance comparisons between QPSK, 8PSK, 16QAM, 64QAM modulated MIMO-OFDM system under AWGN channel. The simulation is performed in static AWGN channel environments and adopts four kinds of constellation modulation modes of QPSK, 8PSK, 16QAM, and 64QAM, respectively. The interlaced PS is inserted in STBC MIMO-OFDM, SIMO-OFDM and SISO-OFDM systems by comb-type manner. The PS1, PS2, PS3, and PS4 are inserted in the proposed SISO/SIMO/STBC MIMO-OFDM systems.

The profiles for the MIMO/SIMO/SISO-OFDM systems are shown in Table 1. The length of CP occupies 512 subcarriers and the number of subcarriers is $N = 2048$ in the MIMO/SIMO/SISO-OFDM systems. The pilot insertion pattern is comb-type and the pilot value is -1.5166 and 1.5166. The pilot interval could be $n = 2$, $n = 4$, $n = 8$, $n = 20$, $n = 50$, and $n = 100$ in MIMO/SIMO/SISO-OFDM systems, respectively.

5.1 2×2 STBC MIMO-OFDM System

Fig. 6 represents the BER performance of 2×2 STBC MIMO-OFDM system under AWGN. Fig. 6(a) shows the BER performance of QPSK modulated 2×2 STBC MIMO-OFDM system under AWGN inserted by PS1. At the target BER of 10^{-3}, the BER curve of STBC MIMO-OFDM system of $n = 100$ outperforms the QPSK BER curves of $n = 50$, $n = 20$, $n = 8$, $n = 4$, and $n = 2$ about 0.05 dB, 0.1 dB, 0.5 dB, 1.2 dB, and 2 dB SNR gains, respectively. Fig. 6(b) shows the BER performance of 8PSK modulated 2×2 STBC MIMO-OFDM system under AWGN inserted by PS3. The 8PSK BER curve of $n = 100$ outperforms the BER curves of $n = 50$, $n = 20$, $n = 8$, $n = 4$, and $n = 2$ about 0.2 dB, 0.35 dB, 1.2 dB, 1.85 dB, and 3.15 dB SNR gains at the target BER of 3×10^{-4}, respectively.

Fig. 6(c) shows the BER performance of 16QAM modulated 2×2 STBC MIMO-OFDM system under AWGN inserted by PS2. At the target BER of 2×10^{-3}, the BER curve of $n = 100$ outperforms the 16QAM BER curves of $n = 50$, $n = 20$, $n = 8$, $n = 4$, and $n = 2$ about 0.1 dB, 0.15 dB, 0.6 dB, 1.1 dB, and 1.9 dB SNR gains, respectively. Fig. 6(d) represents the BER performance of 64QAM modulated 2×2 STBC MIMO-OFDM system under AWGN inserted by PS4. The 64QAM BER curves of $n = 4$, $n = 8$, $n = 20$, $n = 50$, and $n = 100$ outperform the 64QAM BER curve of $n = 2$ about 1.1 dB, 1.9 dB, 1.95 dB, 2.05 dB, and 2.1 dB SNR gains at the target BER of 10^{-3}, respectively.

Fig. 7 represents the BER performances of 2×2 STBC MIMO-OFDM system under one path Rayleigh fading channel. Fig. 7(a) and (b) represent the BER performance of QPSK and 8PSK modulated STBC MIMO-OFDM system under 1 path Rayleigh fading channel. We can see from Fig. 7(a) that when $\text{SNR} = 10\,\text{dB}$, the BER value of $f_\text{d} = 20\,\text{Hz}$, and $f_\text{d} = 60\,\text{Hz}$ becomes zero, but the QPSK BER value of $f_\text{d} = 80$ Hz is 8×10^{-6}. As illustrated in Fig. 7(b), at the target BER of 5×10^{-6}, the 8PSK BER curve of $f_\text{d} = 60\,\text{Hz}$ outperforms the BER curve of $f_\text{d} = 80\,\text{Hz}$, and $f_\text{d} = 20\,\text{Hz}$ about 0.4 dB and 0.8 dB SNR gains. Therefore, the interlaced PS1 and PS4 in QPSK and 8PSK modulated MIMO-OFDM systems could improve the accuracy of channel estimation at the receiver of MIMO-OFDM systems.

Fig. 7(c) and (d) represent the BER performance of 16QAM and 64QAM modulated 2×2 STBC MIMO-OFDM system under one path Rayleigh fading channel. As can be seen from Fig. 7(c), because of the orthogonality of interlaced PS2 in MIMO-OFDM systems with two transmit antennas and two receive antennas, the 16QAM BER curves of $f_\text{d} = 20\,\text{Hz}$, $f_\text{d} = 60\,\text{Hz}$, and $f_\text{d} = 80\,\text{Hz}$ almost have the same performance and at $\text{SNR} = 15\,\text{dB}$, the 16QAM BER value could reach 1.5×10^{-4}. Additionally, at $\text{SNR} = 16\,\text{dB}$, the 16QAM BER curves of $f_\text{d} = 20\,\text{Hz}$, $f_\text{d} = 60\,\text{Hz}$, and $f_\text{d} = 80\,\text{Hz}$ could reach 2.5×10^{-5}, which increases the communication performance of STBC MIMO-OFDM system significantly.

As shown in Fig. 7(d), when the BER is 10^{-3}, the 64QAM BER curves with $f_\text{d} = 20\,\text{Hz}$, $f_\text{d} = 60\,\text{Hz}$, and $f_\text{d} = 80\,\text{Hz}$ almost have the same performance. At $\text{SNR} = 20\,\text{dB}$, the 64QAM BER value of the three curves is 5.6×10^{-4}. It could be concluded that the interlaced PS3 could resist the deep fading interference among different transmit antennas and receive antennas in one path Rayleigh fading channel.

5.2 1×2, 1×3, 1×4, 1×10, 1×20, 1×50, 1×100, 1×200, AND 1×500 SIMO-OFDM System

Fig. 8 represents the BER performance of 1×2 STBC SIMO-OFDM system under AWGN. Fig. 8(a) represents the BER performance of BPSK modulated 1×2 STBC SIMO-OFDM system under AWGN inserted by PS2. At the target BER of 5×10^{-5}, the BER curve of $n=50$ outperforms the $n=100$, $n=20$, $n=8$, $n=4$, and $n=2$ about 0.1 dB, 0.3 dB, 0.8 dB, 1.05 dB, 2.1 dB SNR gains, respectively.

Fig. 8(b) represents the BER performance of QPSK modulated 1×2 STBC SIMO-OFDM system under AWGN inserted by PS1. At the target BER of 4×10^{-5}, the QPSK BER curve of $n=100$ outperforms the BER curves of $n=50$, $n=20$, $n=8$, $n=4$, and $n=2$ about 0.2 dB, 0.3 dB, 0.9 dB, 1.1 dB, and 2.05 dB SNR gains, respectively.

Fig. 8(c) represents the BER performance of QPSK modulated 1×2 SIMO-OFDM system under AWGN inserted by PS3. At the target BER of 3×10^{-5}, the QPSK BER curve of $n=50$ outperforms the BER curves of $n=100$, $n=20$, $n=8$, $n=4$, and $n=2$ could provide about 0.2 dB, 0.4 dB, 0.5 dB, 1.5 dB, and 3.8 dB SNR gains, respectively.

Fig. 8(d) represents the BER performance of 16QAM modulated 1×2 SIMO-OFDM system under AWGN inserted by PS2. At the target BER of 5×10^{-5}, the 16QAM BER curve of $n=100$ outperforms the BER curves of $n=20$, $n=8$, $n=4$, and $n=2$ about 0.4 dB, 0.6 dB, 0.8 dB, and 2.2 dB SNR gains. Fig. 8(e) represents the BER performances of 64QAM modulated 1×2 SIMO-OFDM system under AWGN inserted by PS4. At the target BER of 10^{-5}, the 64QAM BER curve of $n=100$ outperforms the BER curves of $n=20$, $n=8$, $n=4$, and $n=2$ about 0.07 dB, 0.21 dB, 1.35 dB, and 2.25 dB SNR gains, respectively.

Fig. 9 represents the BER performances of 1×3 SIMO-OFDM system under AWGN. Fig. 9(a) represents the BER performance of BPSK modulated 1×3 SIMO-OFDM system under AWGN inserted by PS2. At the target BER of 10^{-4}, the E_b/N_0 gap between BPSK modulation curves of $n=100$ and $n=50$ is 0.05 dB, the E_b/N_0 gap between BPSK modulation curves of $n=50$ and $n=20$ is 0.2 dB, the E_b/N_0 gap between BPSK modulation curves of $n=20$ and $n=8$ is 0.5 dB, the E_b/N_0 gap between BPSK modulation curves of $n=8$ and $n=4$ is 0.6 dB and the E_b/N_0 gap between BPSK modulation curves of $n=4$ and $n=2$ is 0.75 dB. Fig. 9(b) represents the BER performance of QPSK modulated 1×3 SIMO-OFDM system under AWGN inserted by PS1. At the target BER of 10^{-5}, the E_b/N_0 gap between QPSK modulation curves of $n=50$ and $n=100$ is 0.2 dB, the E_b/N_0 gap between QPSK modulation curves of $n=100$ and $n=20$ is 0.4 dB, the E_b/N_0 gap between QPSK modulation curves of $n=20$ and $n=8$ is 0.9 dB, the E_b/N_0 gap between QPSK modulation curves of $n=8$ and $n=4$ is 1.15 dB and the E_b/N_0 gap between QPSK modulation curves of $n=4$ and $n=2$ is 2.15 dB. Fig. 9(c) represents the BER performances of 16QAM modulated 1×3 SIMO-OFDM system under AWGN inserted by PS2. At the target BER of 3×10^{-5}, the 16QAM BER curve of $n=100$ and $n=50$ outperforms the BER curves of $n=20$, $n=8$, $n=4$, and $n=2$ about 0.2 dB, 0.4 dB, 0.6 dB, and 2.1 dB SNR gains, respectively.

Fig. 10 represents the BER performance of 1×4, 1×10, and 1×20 SIMO-OFDM system under AWGN. Fig. 10(a) represents the BER performance of BPSK modulated 1×20 SIMO-OFDM system under AWGN inserted by PS2. At the target BER of 10^{-4}, the BPSK BER curve of $n=100$ outperforms the BPSK BER curves of $n=50$, $n=20$, $n=8$, $n=4$, and $n=2$ about 0.15 dB, 0.25 dB, 0.78 dB, 1.15 dB, and 2.15 dB SNR gains, respectively. Fig. 10(b) represents the BER performance of QPSK modulated 1×10 SIMO-OFDM system under AWGN inserted by PS1. At the target BER of 2×10^{-5}, compared with the QPSK BER curve of $n=100$, the QPSK BER curves of $n=50$, $n=20$, $n=8$, $n=4$, and $n=2$ could provide about 0.7 dB, 0.9 dB, 1.07 dB, 1.9 dB, and 2.02 dB SNR gains, respectively.

Fig. 10(c) represents the BER performance of 8PSK modulated 1×10 SIMO-OFDM system under AWGN inserted by PS2. At the target BER of 10^{-5}, the 8PSK BER curve of $n=100$ outperforms the 8PSK BER curves of $n=50$, $n=20$, $n=8$, $n=4$, and $n=2$ about 0.15 dB, 0.35 dB, 0.85 dB, 1.25 dB, and 3.15 dB SNR gains, respectively.

Fig. 10(d) represents the BER performance of 64QAM modulated 1×4 SIMO-OFDM system under AWGN inserted by PS2. At the target BER of 10^{-4}, the 64QAM BER curves of $n=100$ and $n=50$ outperforms the 64QAM BER curves of $n=20$, $n=8$, $n=4$, and $n=2$ about 0.45 dB, 0.95 dB, 1.25 dB, and 2.65 dB SNR gains, respectively. Fig. 10(e) represents the BER performance of 64QAM modulated 1×20 SIMO-OFDM system under AWGN inserted by PS4. At the target BER of 3×10^{-5}, the 64QAM BER curve of $n=100$ outperforms the 64QAM BER curves of $n=50$, $n=20$, $n=8$, $n=4$, and $n=2$ about 0.08 dB, 0.09 dB, 1.15 dB, 1.85 dB, and 3.25 dB SNR gains, respectively.

Fig. 11 represents the BER performance of 1×50 SIMO-OFDM system under AWGN. Fig. 11(a) shows the BPSK modulated 1×50 SIMO-OFDM system under AWGN inserted by PS4. At the target BER of 10^{-5}, the E_b/N_0 gaps among $n=100$, $n=8$, $n=4$, and $n=2$ are 0.7 dB, 0.8 dB, and 1.35 dB. Fig. 11(b) shows the

QPSK modulated 1×50 SIMO-OFDM system under AWGN inserted by PS1. At the target BER of 10^{-5}, the QPSK BER curve of $n=100$ outperforms the QPSK BER curves of $n=50$, $n=20$, $n=8$, $n=4$, and $n=2$ about 0.2 dB, 0.4 dB, 0.7 dB, 1.6 dB, and 2.3 dB SNR gains, respectively. Fig. 11(c) illustrates the 16QAM modulated 1×50 SIMO-OFDM system under AWGN inserted by PS2. At the target BER of 10^{-4}, compared with the 16QAM BER curves of $n=50$, $n=20$, $n=8$, $n=4$, and $n=2$, the BER curve of $n=100$ could provide about 0.1 dB, 0.2 dB, 0.7 dB, 1.1 dB, and 2.1 dB SNR gains, respectively.

Fig. 12 represents the BER performance of 1×100 SIMO-OFDM system under AWGN. Fig. 12(a) shows the BER performance of BPSK modulated 1×100 SIMO-OFDM system under AWGN inserted by PS1. At the target BER of 10^{-4}, compared with the BPSK BER curves of $n=50$, $n=20$, $n=8$, $n=4$, and $n=2$, the BPSK BER curve of $n=100$ could provide about 0.2 dB, 0.8 dB, 0.9 dB, 1.4 dB, and 2.3 dB SNR gains, respectively. Fig. 12(b) shows the BER performance of 8PSK modulated 1×100 SIMO-OFDM system under AWGN inserted by PS1. At the target BER of 7×10^{-5}, compared with the 8PSK BER curve of the $n=100$, the 8PSK BER curves of $n=50$, $n=20$, $n=8$, $n=4$, and $n=2$ could provide about 0.15 dB, 0.28 dB, 0.83 dB, 1.11 dB, and 2.08 dB SNR degradation, respectively. Fig. 12(c) illustrates the BER performance of 64QAM modulated 1×100 SIMO-OFDM system under AWGN inserted by PS3. At the target BER of 10^{-4}, compared with the 64QAM BER curves of $n=50$, $n=20$, $n=8$, $n=4$, and $n=2$, the 64QAM BER curve of $n=100$ could provide about 0.1 dB, 0.2 dB, 0.7 dB, 1.1 dB, and 2.1 dB SNR gains, respectively.

Fig. 13 represents the BER performance of 1×200 SIMO-OFDM system under AWGN. Fig. 13(a) represents the BER performance of BPSK modulated 1×200 SIMO-OFDM system under AWGN inserted by PS1. At the target BER of 5×10^{-5}, compared with the BPSK BER curve of $n=2$, the BPSK BER curves of $n=50$, $n=20$, $n=100$, $n=8$, and $n=4$ could provide about 2.05 dB, 1.95 dB, 1.85 dB, 1.65 dB, and 0.95 dB SNR gains, respectively. Fig. 13(b) represents the BER performance of 8PSK modulated 1×200 SIMO-OFDM system under AWGN inserted by PS2. At the target BER of 10^{-5}, compared with the 8PSK BER curve of the $n=2$, the 8PSK BER curves of $n=100$, $n=20$, $n=8$, and $n=4$ could provide about 2.1 dB, 2.05 dB, 1.25 dB, and 1.05 dB SNR degradation, respectively. Fig. 13(c) illustrates the BER performance of 16QAM modulated 1×200 SIMO-OFDM system under AWGN inserted by PS3. At the target BER of 10^{-4}, compared with the 16QAM BER curve of $n=2$, the 16QAM BER curves of $n=100$, $n=50$, $n=20$, $n=8$, and $n=4$ could provide about 2.7 dB, 2.6 dB, 2.4 dB, 2.1 dB, and 0.9 dB SNR gains, respectively.

Fig. 14 represents the BER performance of 1×500 SIMO-OFDM system under AWGN. Fig. 14(a) illustrates the BER performance of BPSK modulated 1×500 SIMO-OFDM system under AWGN inserted by PS3. At the target BER of 3×10^{-5}, compared with the 8PSK BER curve of $n=2$, the 8PSK BER curves of $n=4$, $n=8$, $n=100$, and $n=50$ could provide about 1.5 dB, 2.1 dB, 2.3 dB, and 2.4 dB SNR gains, respectively. Fig. 14(b) represents the BER performance of QPSK modulated 1×500 SIMO-OFDM system under AWGN inserted by PS1. At the target BER of 4×10^{-5}, compared with the QPSK BER curves of $n=100$, the QPSK BER curves of $n=50$, $n=20$, $n=8$, $n=4$, and $n=2$ could lose about 0.8 dB, 1.1 dB, 1.3 dB, 1.5 dB, and 2.2 dB SNR, respectively. Fig. 14(c) represents the BER performance of 64QAM modulated 1×500 SIMO-OFDM system under AWGN inserted by PS2. At the target BER of 3×10^{-5}, compared with the 64QAM BER curve of the $n=2$, the 64QAM BER curves of $n=4$, $n=8$, $n=20$, $n=50$, and $n=100$ have about 0.75 dB, 2.1 dB, 2.2 dB, 2.25 dB, and 2.3 dB SNR degradation, respectively.

5.3 1×1 SISO-OFDM System

Fig. 15 represents the BER performance of 1×1 SISO-OFDM system under AWGN. Fig. 15(a) represents the BER performance of BPSK modulated SISO-OFDM system under AWGN inserted by PS1. At the target BER of 10^{-4}, the BPSK BER curves of $n=100$ and $n=50$ outperform the BPSK BER curves of $n=20$, $n=8$, $n=4$, and $n=2$ about 0.2 dB, 0.6 dB, 1.05 dB, and 2.1 dB SNR gains, respectively.

Fig. 15(b) illustrates the BER performance of 8PSK modulated 1×1 SISO-OFDM system under AWGN inserted by PS1. At the target BER of 10^{-4}, compared with the 8PSK BER curves of $n=50$, $n=20$, $n=8$, $n=4$, and $n=2$, the 8PSK BER curve of $n=100$ could provide about 0.1 dB, 0.2 dB, 0.7 dB, 1.1 dB, and 2.1 dB SNR gains, respectively. Fig. 15(c) represents the BER performance of QPSK modulated SISO-OFDM system under AWGN inserted by PS3. At the target BER of 10^{-5}, the QPSK BER curve of $n=100$ outperforms the QPSK BER curves of $n=50$, $n=20$, $n=8$, $n=4$, and $n=2$ about 0.2 dB, 0.4 dB, 1.1 dB, 1.5 dB, and 2.15 dB SNR gains, respectively.

Fig. 16 represents the BER performance of 1×1 SISO-OFDM system under AWGN. Fig. 16(a) represents the BER performance of BPSK modulated SISO-OFDM system under AWGN inserted by PS3. At the target BER of 10^{-4}, the BPSK BER curve of $n=100$ outperforms the BPSK BER curves of $n=50$, $n=20$, $n=8$, $n=4$, and $n=2$ about 0.1 dB, 0.2 dB, 0.5 dB, 1.1 dB, and 2.3 dB SNR gains, respectively.

Fig. 16(b) represents the BER performance of 64QAM modulated SISO-OFDM system under AWGN inserted by PS2. At the target BER of 10^{-5}, the 64QAM BER curve of $n=100$ outperforms the 64QAM BER curves of $n=50$, $n=8$, and $n=4$ about 0.4 dB, 0.6 dB, and 1.45 dB SNR gains, respectively. Fig. 16(c) represents the BER performance of 64QAM modulated SISO-OFDM system under AWGN by inserted PS4. At the target BER of 10^{-5}, the 64QAM BER curve of $n=100$ outperforms the 64QAM BER curves of $n=50$, $n=20$, $n=8$, $n=4$, and $n=2$ about 0.2 dB, 0.26 dB, 1.12 dB, 1.78 dB, and 2.89 dB SNR gains, respectively.

6. Conclusion

In this paper, four optimal pilot patterns for 2×2 STBC MIMO-OFDM, 1×2, 1×3, 1×4, 1×10, 1×20, 1×50, 1×100, 1×200, and 1×500 SIMO-OFDM, and 1×1 SISO-OFDM systems are studied. This paper proposed new pilot patterns to estimate the transmitted OFDM symbols by effectively allocate pilot sequences through frequency resources. STBC pilot pattern works well for both 2×2 STBC MIMO-OFDM, 1×2, 1×3, 1×4, 1×10, 1×20, 1×50, 1×100, 1×200, and 1×500 SIMO-OFDM, and SISO-OFDM systems. The proposed optimal pilot patterns eliminate the drawbacks of STBC and conventional pilot patterns. The performance of MIMO/SIMO/SISO-OFDM systems is improved as can be observed from the simulation results.

In the future, we will apply the proposed pilot sequence assisted channel estimation method in cognitive MIMO-OFDM system [31]–[33], massive SIMO-OFDM systems, UWB MIMO-OFDM systems [34], CMMB MIMO-OFDM systems [35], massive MIMO-OFDM systems [36]–[40] and underwater acoustic OFDM systems [41].

Abbreviation
BPSK: binary phase shift keying
BS: base stations
CSI: channel state information
ICI: inter-carrier interference
IFFT: inverse fast Fourier transform
LOS: light of sight
LS: least square
MIMO: multiple input multiple output
MSE: mean square error
OFDM: orthogonal frequency division multiplexing
OTS: optimal training sequences
PDF: power distribution function
QPSK: quadrature phase shift keying
QAM: quadrature amplitude modulation
SISO: single input single output
SIMO: single input multiple output
STBC: space time block coding

Declarations

Acknowledgements
The authors thank Mingtong Zhang and Ruiguang Tang for their kind help and valuable suggestions in revising this paper.

Funding
This work was supported in part by the National Natural Science Foundation of China under Grant no. 61702303, in part by the Shandong Provincial Natural Science Foundation, China under Grant no. ZR2017MF020, and in part by the Science and Technology Development Plan Project of Weihai Municipality under Grant no. 2019DXGJ12.

Availability of data and materials
Not applicable.

Authors' contributions

Xiao Zhou and Chengyou Wang conceived the algorithm and designed the experiments; Chengyou Wang performed the experiments; Xiao Zhou analyzed the results; Xiao Zhou and Chengyou Wang drafted the manuscript; Xiao Zhou and Qun Wu revised the manuscript. All authors read and approved the final manuscript.

Competing interests
The authors declare that they have no competing interests.

Authors' information
Xiao Zhou received her B.E. degree in automation from Nanjing University of Posts and Telecommunications, China, in 2003; her M.E. degree in information and communication engineering from Inha University, Korea, in 2005; and her Ph.D. degree in information and communication engineering from Tsinghua University, China, in 2013. She is currently a lecturer and supervisor of postgraduate students at Shandong University, Weihai, China. Her current research interests include wireless communication technology, digital image processing, and computer vision.

Chengyou Wang received his B.E. degree in electronic information science and technology from Yantai University, China, in 2004, and his M.E. and Ph.D. degrees in signal and information processing from Tianjin University, China, in 2007 and 2010, respectively. He is currently an associate professor and supervisor of postgraduate students at Shandong University, Weihai, China. His current research interests include digital image/video processing and analysis, computer vision, machine learning, and wireless communication technology.

Qun Wu was born in Heze city, Shandong province, China, in 1998. She received the B.E. degree in electronic information engineering from Jiangxi University of Science and Technology, China, in 2020. She is currently pursuing the M.E. degree in information and communication engineering at Shandong University, China. Her current research interests include wireless communication theory and technology and computer vision.

References

[1] F Adachi, A Bookajay, T Saito, Y Seki, Performance comparison of MIMO diversity schemes in a frequency-selective Rayleigh fading channel. In: Proc. of the Int. Conf. Commun. Sys., Chengdu, China, pp. 62–66 (2018)
[2] J Zheng, R. Chen, Achieving transmit diversity in OFDM-IM by utilizing multiple signal constellations. IEEE Access, **5**, 8978–8988 (2017)
[3] CB Papadias, GJ Foschini, A space-time coding approach for systems employing four transmit antennas. In: Proc. of the IEEE Int. Conf. Acoustics, Speech and Signal Proc., Salt Lake, UT, USA, vol. 4, pp. 2481–2484 (2001)
[4] H Huang, H Viswanathan, GJ Foschini, Multiple antennas in cellular CDMA systems: Transmission, detection, and spectral efficiency. IEEE Trans. Wireless Commun., **1**(3), pp. 383–392 (2002)
[5] H Alves, M De Castro Tome, PHJ Nardelli, CHM De Lima, M Latva-Aho, Enhanced transmit antenna selection scheme for secure throughput maximization without CSI at the transmitter. IEEE Access, **4**, pp. 4861–4873 (2016)
[6] K Sagar, P. Palanisamy, Optimal orthogonal pilots design for MIMO-OFDM channel estimation. In: Proc. of the 5th IEEE Int. Conf. Comput. Intell. Comput., Coimbatore, Tamilnadu, India, pp. 1–4 (2014)
[7] P Zhou, CM Zhao, B Sheng, Channel estimation based on pilot-assisted for MIMO-OFDM systems. Journal of Electronics and Information Technology, **29**(1), pp. 133–137 (2007)
[8] X Geng, H Hu, W Cui, Y Dun, Optimal pilot design for MIMO OFDM channel estimation. In: Proc. of the 2nd Int. Conf. Signal Proc. Sys., Dalian, China, vol. 2, pp. 2404–2408 (2010)
[9] JW Kang, Y Whang, HY Lee, KS Kim, Optimal pilot sequences design for multi-cell MIMO-OFDM systems. IEEE Trans. Wireless Commun., **10**(10), pp. 3354–3367 (2011)
[10] H Al-Salih, MR Nakhai, TA Le, Enhanced sparse Bayesian learning-based channel estimation with optimal pilot design for massive MIMO-OFDM systems. IET Commun., **12**(17), pp. 2174–2180 (2018)
[11] SJ Chern, YS Huang, YG Jan, RHH Yang, Performance of the MIMO PRCP-OFDM system with orthogonal cyclic-shift sequences. In: Proc. of the IEEE Int. Symp. Intelligent. Sig. Proc. Commun. Syst., Tamsui, New Taipei City, Taiwan, pp. 553–558 (2012)
[12] JA Del Peral-Rosado, MA Barreto-Arboleda, F Zanier, M Crisci, G Seco-Granados, JA Lopez-Salcedo, Pilot placement for power-efficient uplink positioning in 5G vehicular networks. In: Proc. of the 18th IEEE Int. Workshop Sig. Proc. Advan. Wireless Commun., Sapporo, Japan, pp. 1–5 (2017)
[13] T Younas, J Li, J Arshad, On bandwidth efficiency analysis for LS-MIMO with hardware impairments. IEEE Access, **5**, pp. 5994–6001 (2017).

[14]P Krishna, TA Kumar, KK Rao, Pilot based LMMSE channel estimation for multi-user MIMO-OFDM system with power delay profile. In: Proc. of the IEEE Asia Pacific Conf. Circ. Syst., Ishigaki Island, Okinawa, Japan, pp. 487–490 (2014)
[15]Y Seki, A Boonkajay, F Adachi, Adaptive MMSE-SVD to improve the tracking ability against fast fading. In: Proc. of the IEEE 88th Vehicular Tech. Conf., Chicago, IL, USA, pp. 1–5 (2018)
[16]H Lei, J Zhang, KH Park, P Xu, IS Ansari, G Pan, B Alomair, MS Alouini, On secure NOMA systems with transmit antenna selection schemes. IEEE Access, **5**, pp. 17450–17464 (2017).
[17]Y Seki, F Adachi, Downlink capacity comparison of MMSE-SVD and BD-SVD for cooperative distributed antenna transmission using multi-user scheduling. In: Proc. of the IEEE 86th Vehicular Tech. Conf., Toronto, ON, Canada, pp. 1–5 (2017)
[18]L Wang, Y Kuang, J Liu, Pilot-assistant subcarrier allocation in virtual MISO-OFDM system. In: Proc. of the IEEE 12th Int. Conf. Commun. Tech., Nanjing, China, pp. 713–716 (2010)
[19]MA Youssefi, J El Abbadi, Pilot-symbol patterns for MIMO OFDM systems under time varying channels. In: Proc. of the 1st Int. Conf. Electr. Inf. Technol., Marrakech, Morocco, pp. 322–328 (2015)
[20]F Sun, J Zhang, Y Zhang, C Huang, A novel channel estimation scheme for MIMO-OFDM systems with virtual subcarriers. In: Proc. of the IEEE Veh. Technol. Conf., Marina Bay, Singapore, pp. 928–932 (2008)
[21]W Sun, W Yang, L Li, A simple channel estimation method in MIMO-OFDM systems with virtual subcarriers. In: Proc. of the IEEE Int. Conf. Wirel. Commun., Networking Inf. Secur., Beijing, China, pp. 35–39 (2010)
[22]L Tang, Q Tan, Y Shi, C Wang, Q Chen, Adaptive virtual resource allocation in 5G network slicing using constrained Markov decision process. IEEE Access, **6**, pp. 61184–61195 (2018)
[23]Q Huang, M Ghongho, S Freear, Pilot design for MIMO OFDM systems with virtual carriers. IEEE Trans. Signal Proc., **57**(5), pp. 2024–2029 (2009).
[24]A Kenarsari-Anhari L Lampe, Power allocation for coded OFDM via linear programming. IEEE Commun. Lett., **13**(12), pp. 887–889 (2009)
[25]Z Wang, S Dang, DT Kennedy, Multi-hop index modulation-aided OFDM with decode-and-forward relaying. IEEE Access, **6**, pp. 26457–26468 (2018).
[26]C Poongodi, P Ramya, A Shanmugam, BER analysis of MIMO OFDM system using M-QAM over Rayleigh fading channel. In: Proc. of the Int. Conf. Commun. Comput. Intell., Erode, India, pp. 284–288 (2010)
[27]G Casu, F Georgescu, M Nicolaescu, A Mocanu, A comparative performance analysis of MIMO-OFDM system over different fading channels. In: Proc. of the Int. Conf. Electron., Comput. Artif. Intell., Bucharest, Romania, pp. 1–4 (2015)
[28]SH Aswini, BN Ardra Lekshmi, S Sekhar, SS Pillai, MIMO-OFDM frequency offset estimation for Rayleigh fading channels. In: Proc. of the 1st Int. Conf. Comput. Syst. Commun., Trivandrum, India, pp. 191–196 (2014)
[29]A Albehadili, K Al Shamaileh, A Javaid, J Oluoch, V Devabhaktuni, An upper bound on PHY-layer key generation for secure communications over a Nakagami-M fading channel with asymmetric additive noise. IEEE Access, **6**, pp. 28137–28149 (2018)
[30]Y Wang, H Cao, Capacity bounds for Rayleigh/lognormal MIMO channels with double-sided correlation. IEEE Commun. Letters, **19**(8), pp. 1362–1365 (2015)
[31]DT Ngo, C Tellambura, HH Nguyen, Resource allocation for OFDM-based cognitive radio multicast networks. In: Proc. of the IEEE Wireless Commun. Networking Conf., Budapest, Hungary, pp. 1–6 (2009)
[32]CN Devanarayana, AS Alfa, Decentralized channel assignment and power allocation in a full-duplex cognitive radio network. In: Proc. of the 13th IEEE Annual Consum. Commun. Net. Conf., Las Vegas, NV, USA, pp. 829–832 (2016)
[33]X Zhou, W Xu, X Shi, J Lin, Energy-efficient power loading with intercarrier and intersymbol interference considerations for cognitive OFDM systems. In: Proc. of the IEEE 81st Vehicular Tech. Conf., Glasgow, United Kingdom, pp. 1–5 (2015)
[34]N M Anas, SKS Yusof, R Mohamad, On the performance of SVD estimation in Saleh-Valenzuela channel for UWB systems. In: Proc. of the IEEE Reg. 10 Annu. Int. Conf. Proc., Xi'an, China, pp. 1–5 (2013)
[35]F Hu, Y Wang, L Jin, Robust MIMO-OFDM design for CMMB systems based on LMMSE channel estimation. In: Proc. of the IEEE Int. Conf. Electron. Inf. Emerg. Commun., Beijing, China, pp. 59–62 (2015).
[36]R Kudo, SM Armour, JP McGeehan, M Mizoguchi, A channel state information feedback method for massive MIMO-OFDM. J. Commun. Netw., **15**(4), pp. 352–361 (2013)
[37]J Yuan, H Shan, A Huang, TQS Quek, YD Yao, Massive machine to machine communications in cellular network: Distributed queueing random access meets MIMO. IEEE Access, **5**, pp. 2981–2993 (2017).
[38]K Zhang, W Tan, G Xu, C Yin, W Liu, C Li, Joint RRH activation and robust coordinated beamforming for massive MIMO heterogeneous cloud radio access networks. IEEE Access, **6**, pp. 40506–40518 (2018)

[39]C Xu, Y Hu, C Liang, J Ma, L Ping, Massive MIMO, non-orthogonal multiple access and interleave division multiple access. IEEE Access, **5**, pp. 14728–14748 (2017)
[40]A Mejri, M Hajjaj, S Hasnaoui, R Bouallegue, Singular value thresholding based adaptive approach for hybrid beamforming in MmWave massive MIMO-OFDM transmitters. In Proc. of the 26th Int. Conf. Software, Telecommun. Comput. Networks, Split, Croatia, pp. 207–202 (2018)
[41]R Jiang, X Wang, S Cao, J Zhao, X Li, Deep neural networks for channel estimation in underwater acoustic OFDM systems. IEEE Access, **7**, pp. 23579–23594 (2019)

Tables and Figures

Figures

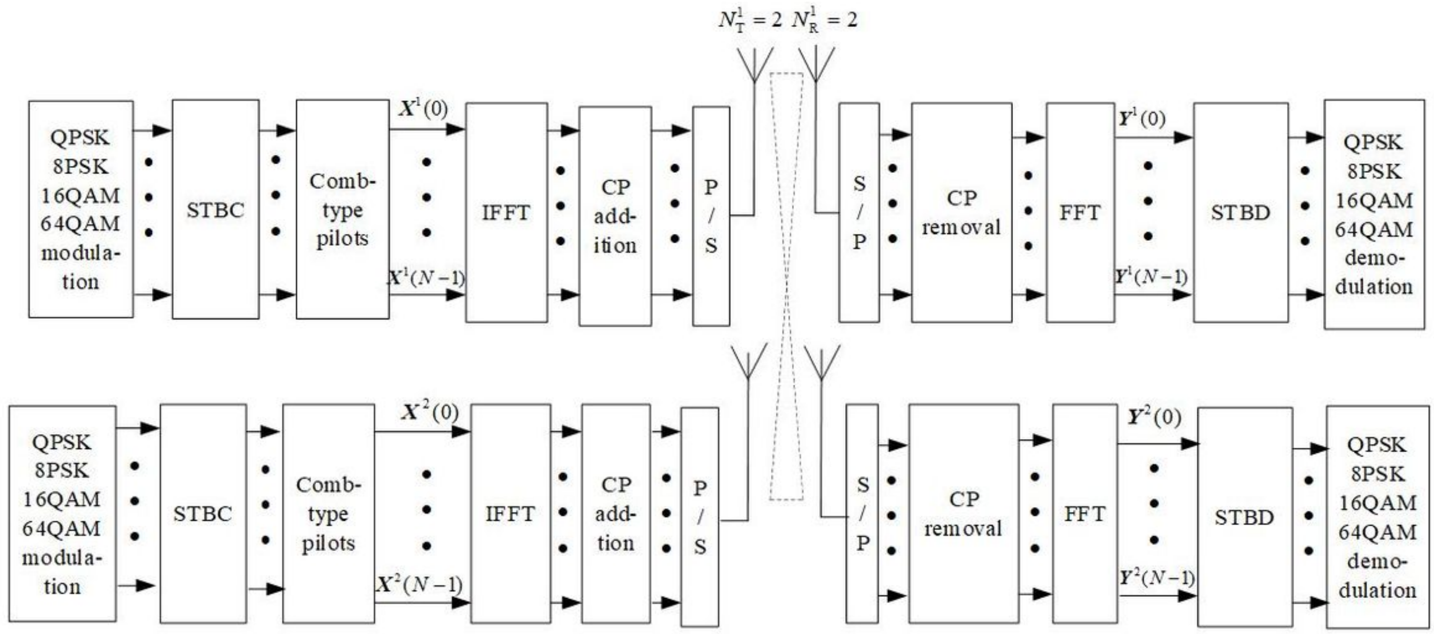

Figure 1

Fig. 1 and Fig. 2 illustrate the MIMO-, and SISO-OFDM systems, respectively. In this paper, we consider the MIMO-OFDM system with the number of transmit and receive antennas , , and SISO-OFDM system with , .

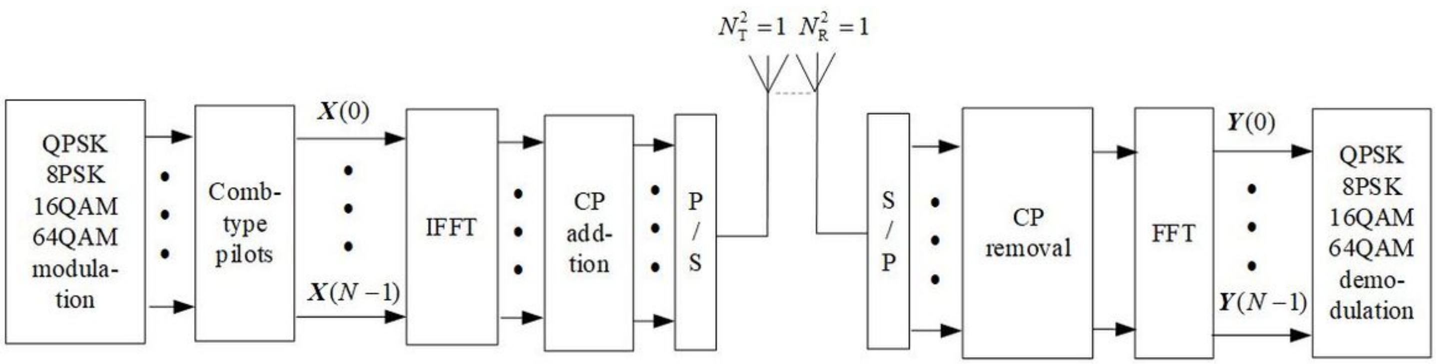

Figure 2

Fig. 1 and Fig. 2 illustrate the MIMO-, and SISO-OFDM systems, respectively. In this paper, we consider the MIMO-OFDM system with the number of transmit and receive antennas , , and SISO-OFDM system with , .

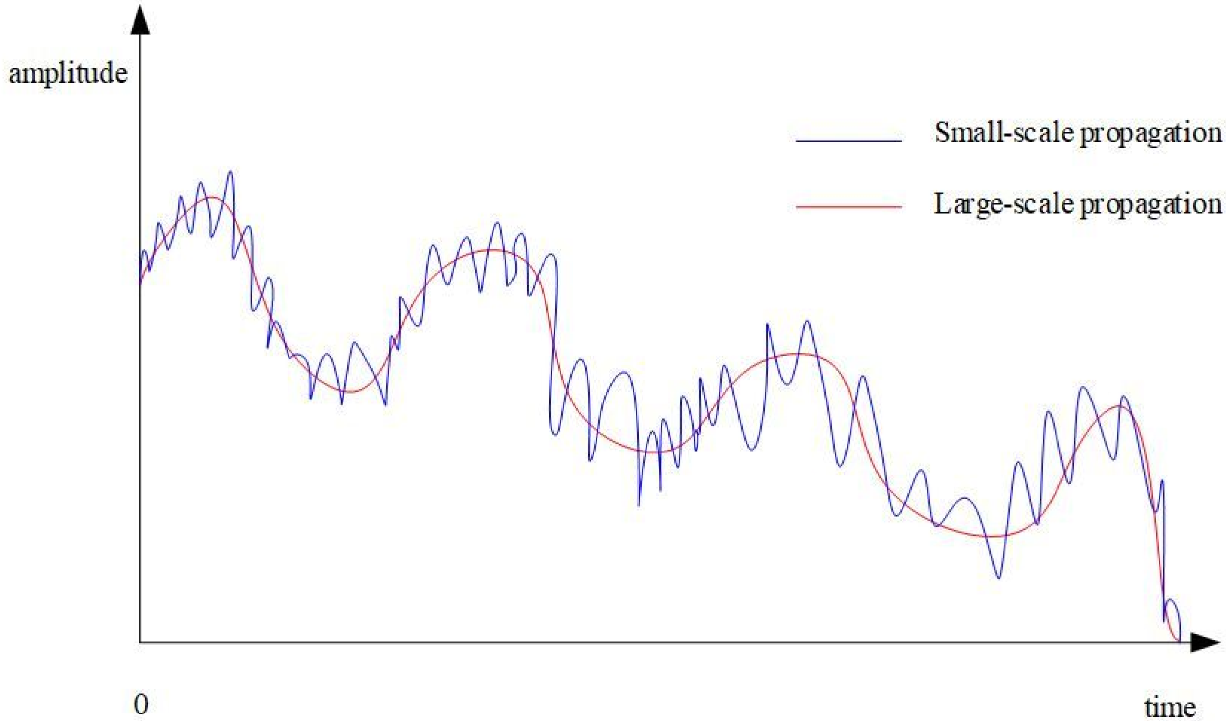

Figure 3

Fig. 3 illustrates large-scale propagation and small-scale propagation of the STBC MIMO-OFDM. When increases, it would induce time selective propagation, which is illustrated in Fig. 3

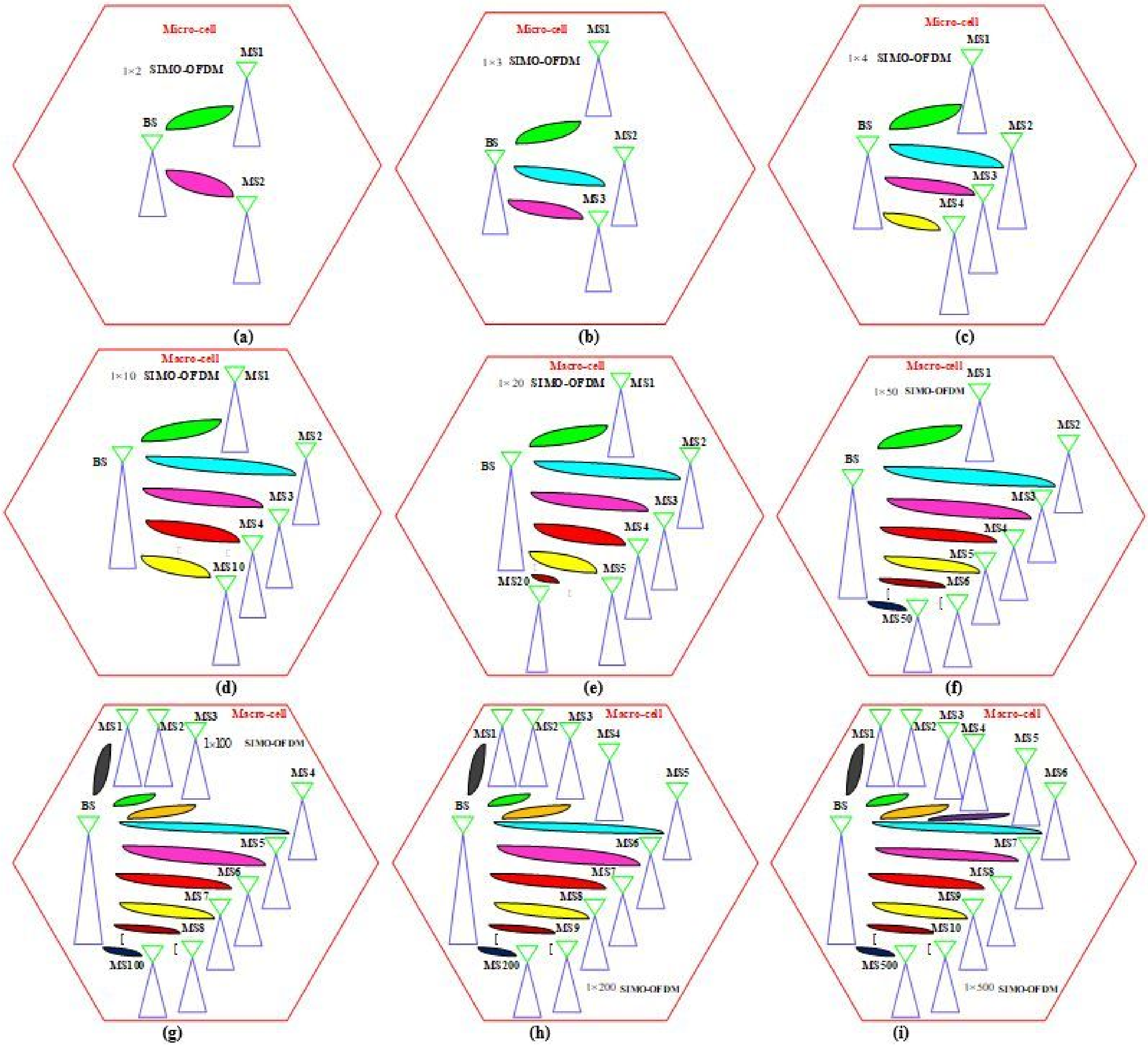

Figure 4

Fig. 4 illustrates SIMO-OFDM models utilized in micro-cell and macro-cell. According to the number of receive antennas, SIMO-OFDM, SIMO-OFDM, SIMO-OFDM could be utilized in micro-cell and SIMO-OFDM, SIMO-OFDM could be utilized in macro-cell

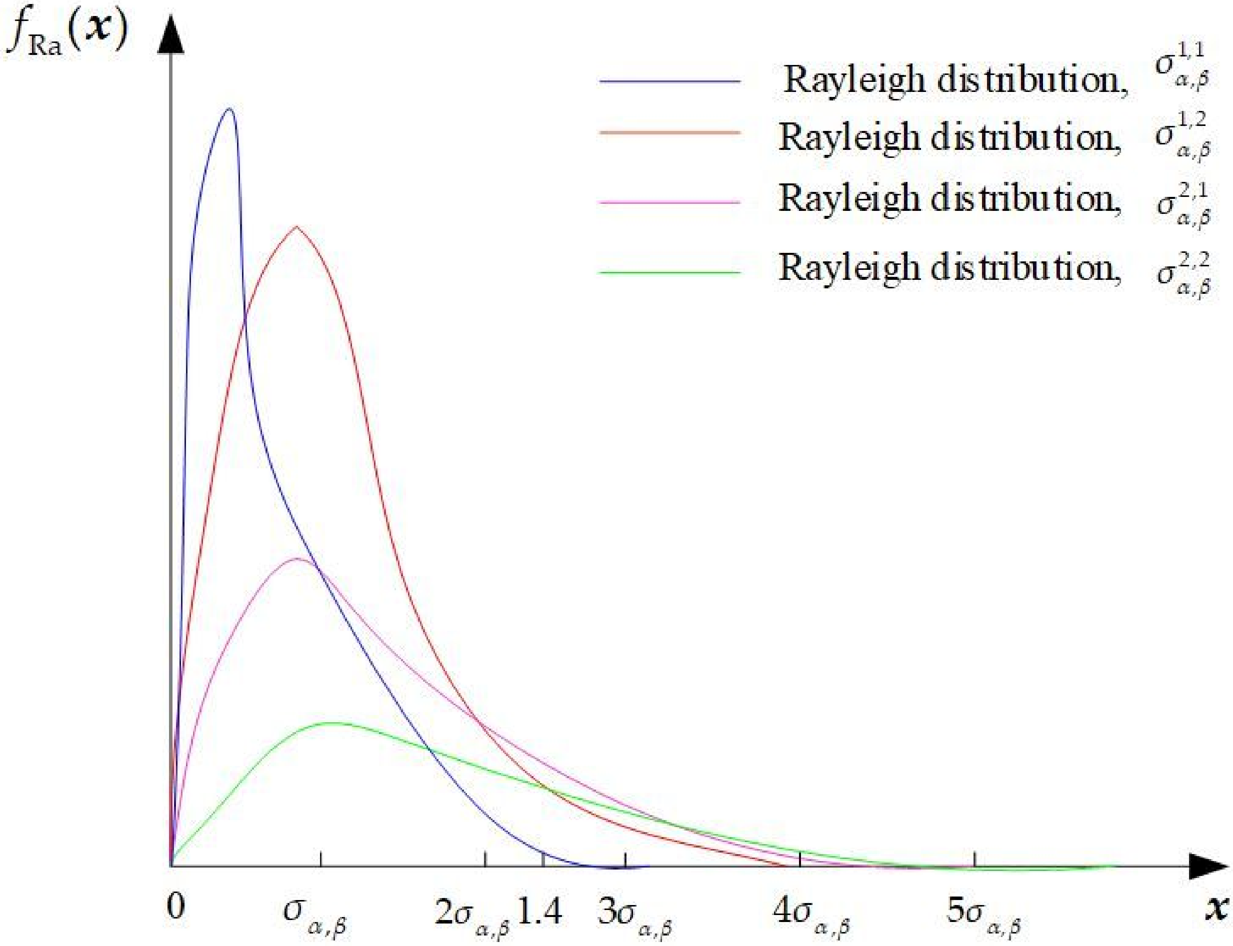

Figure 5

Fig. 5 illustrates the Rayleigh distribution under different noise standard deviation

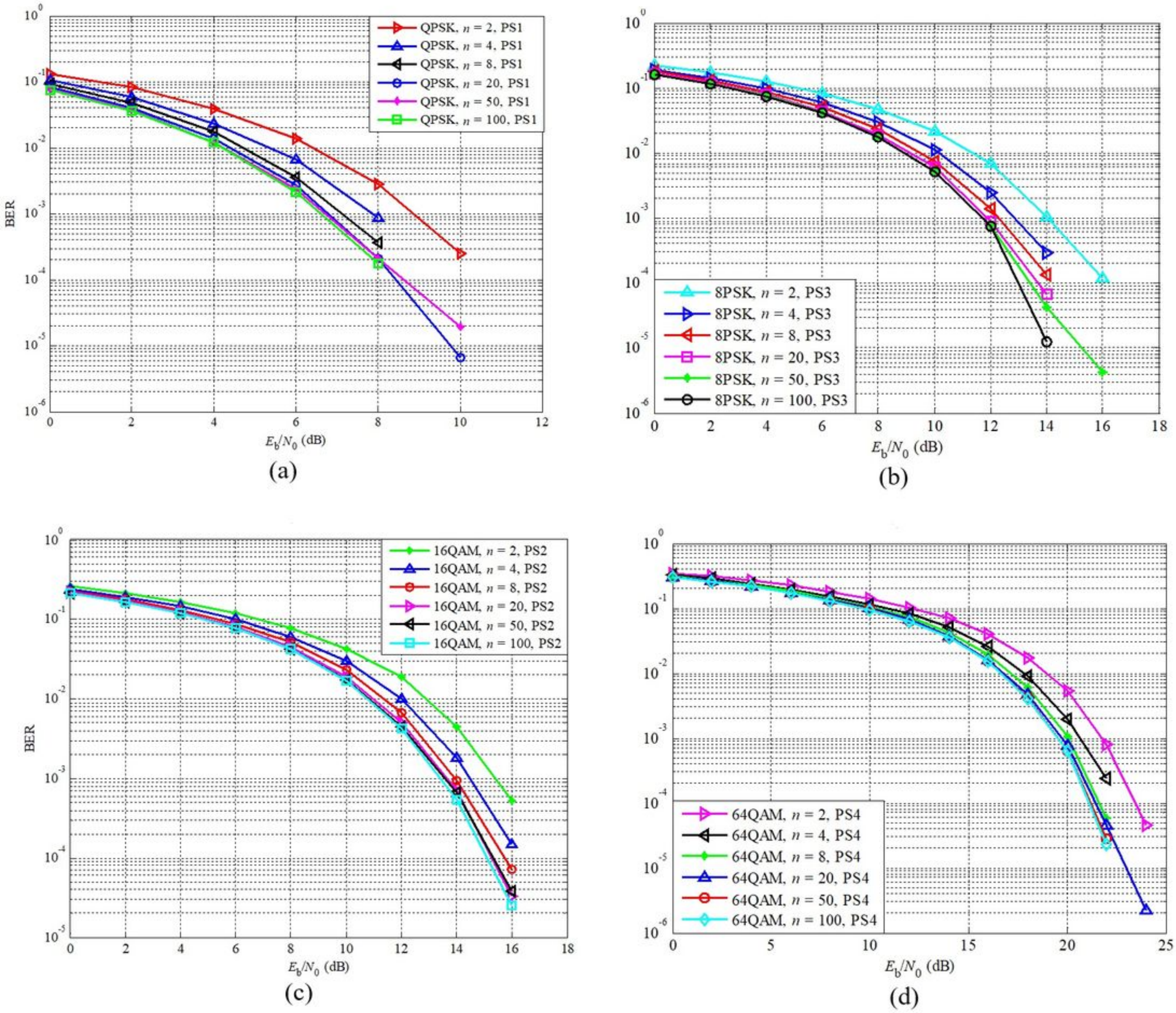

Figure 6

Fig. 6 represents the BER performance of STBC MIMO-OFDM system under AWGN.

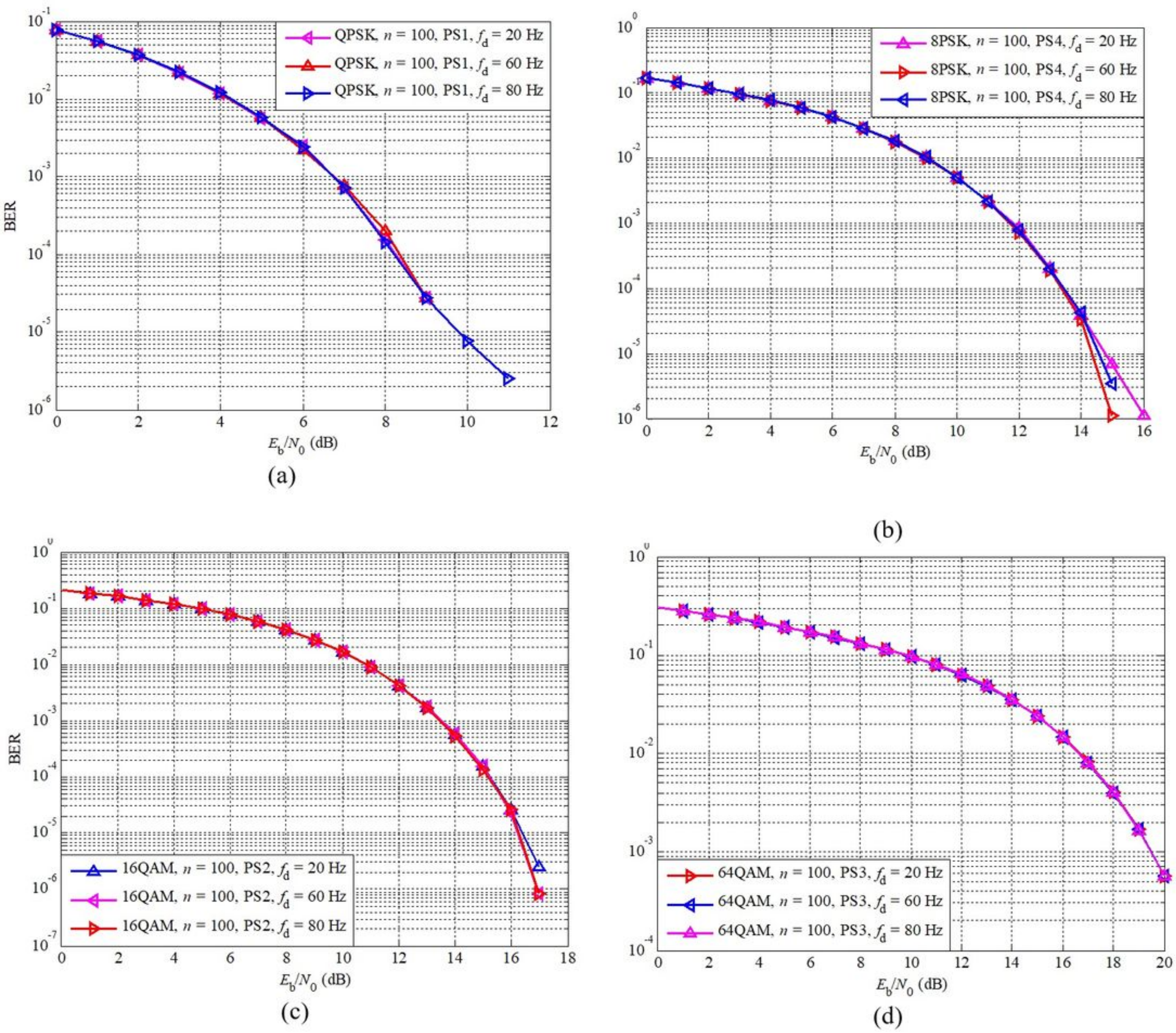

Figure 7

Fig. 7 represents the BER performances of STBC MIMO-OFDM system under one path Rayleigh fading channel.

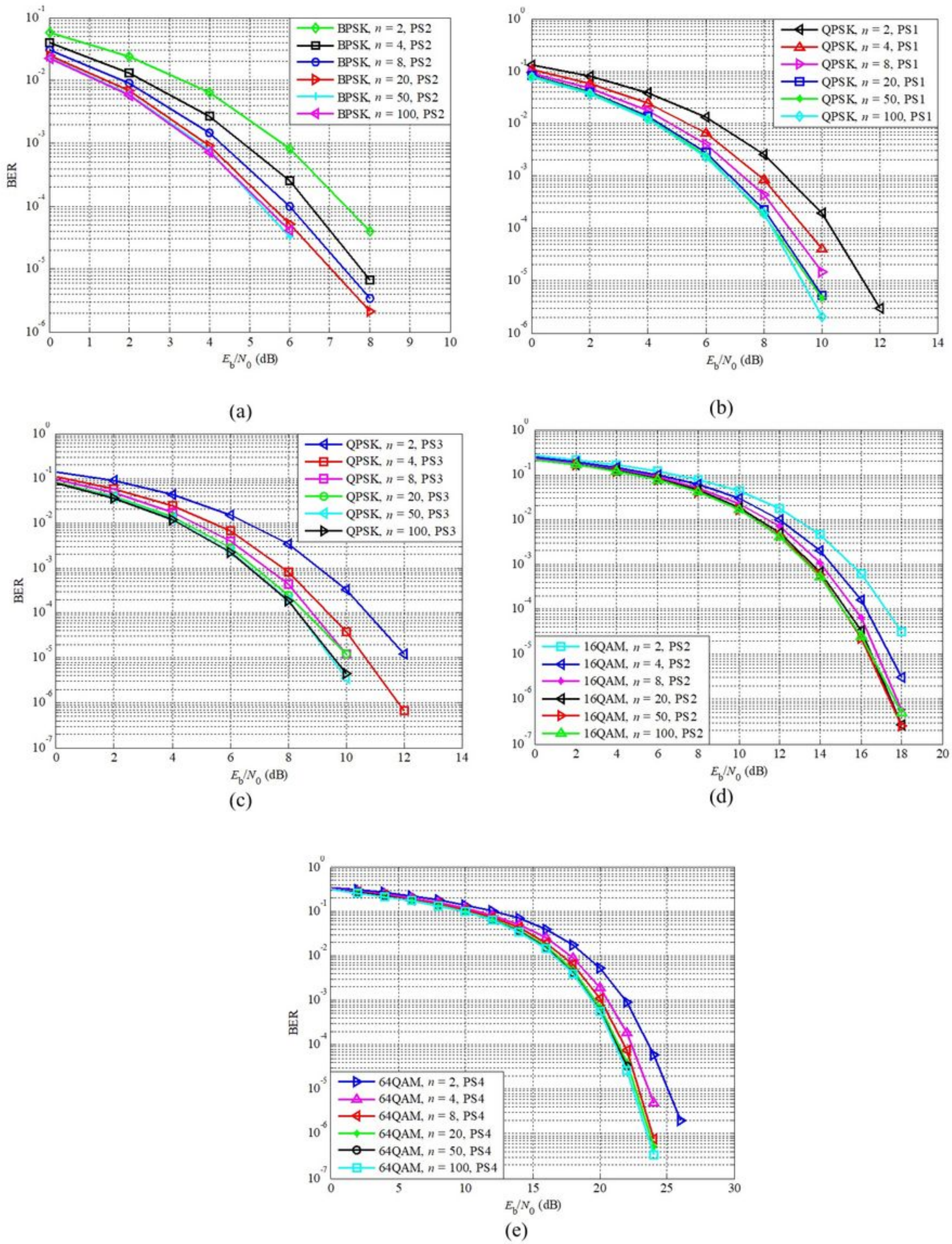

Figure 8

Fig. 8 represents the BER performance of STBC SIMO-OFDM system under AWGN

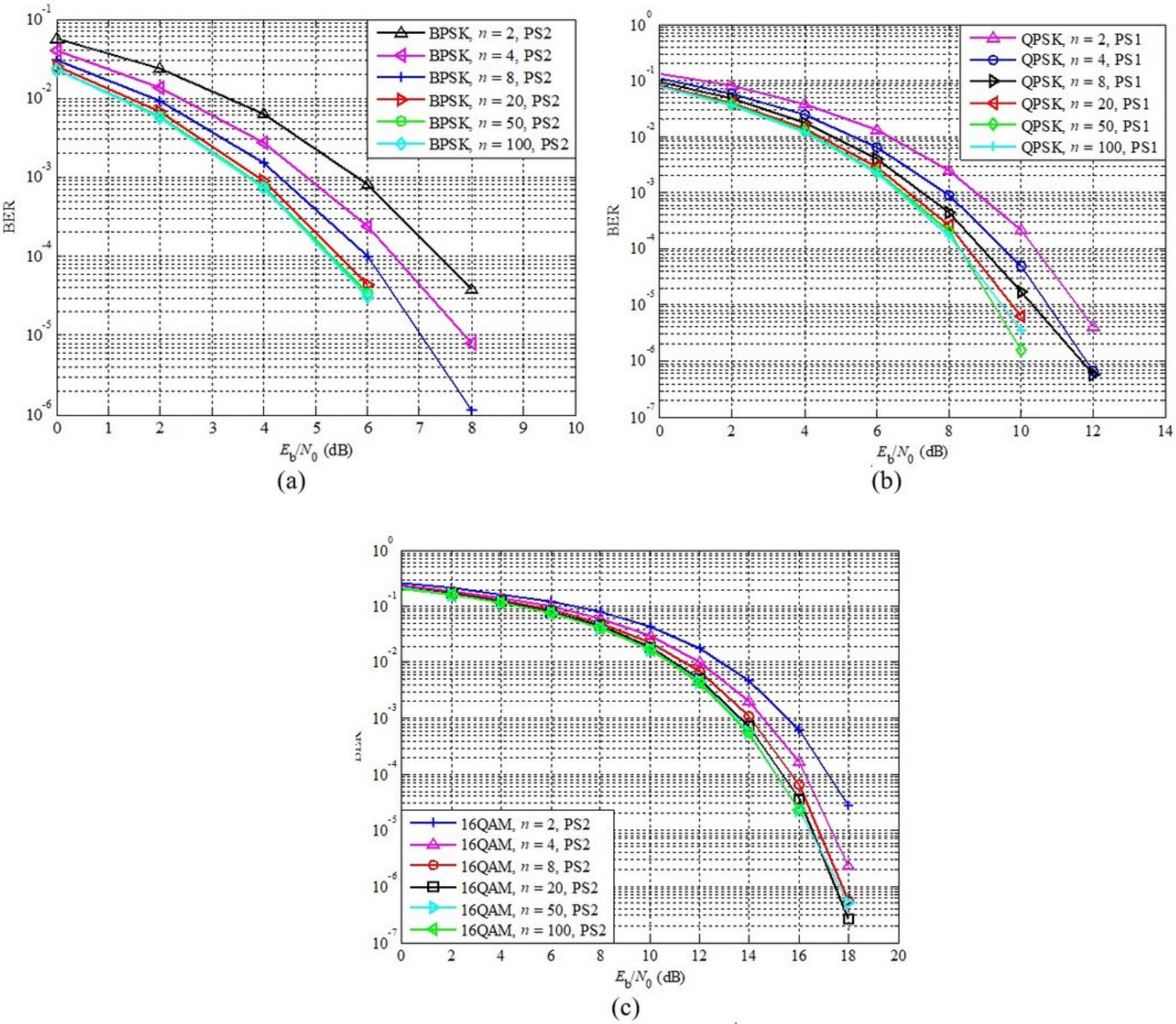

Figure 9

Fig. 9 represents the BER performances of SIMO-OFDM system under AWGN

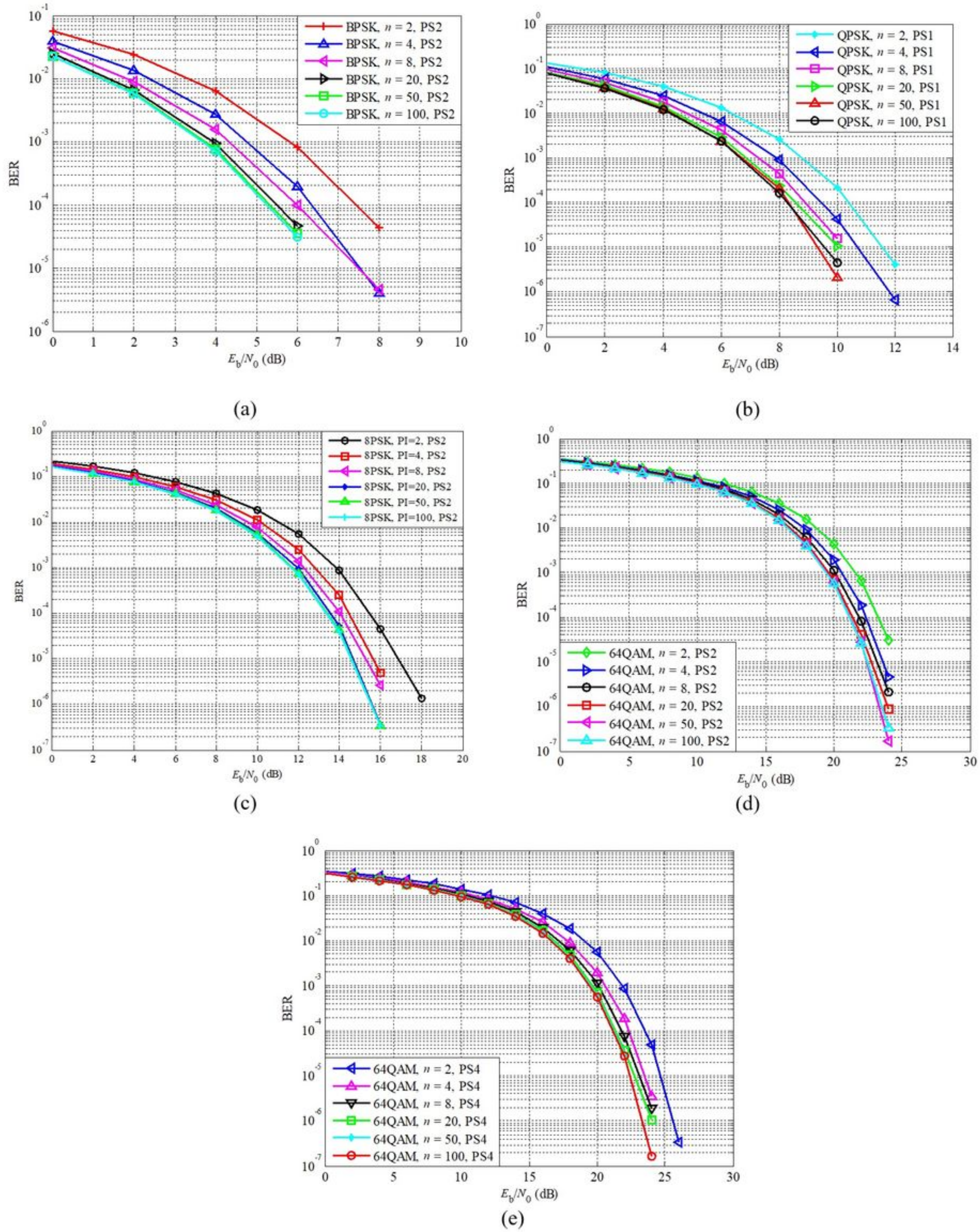

Figure 10

Fig. 10 represents the BER performance of , , and SIMO-OFDM system under AWGN

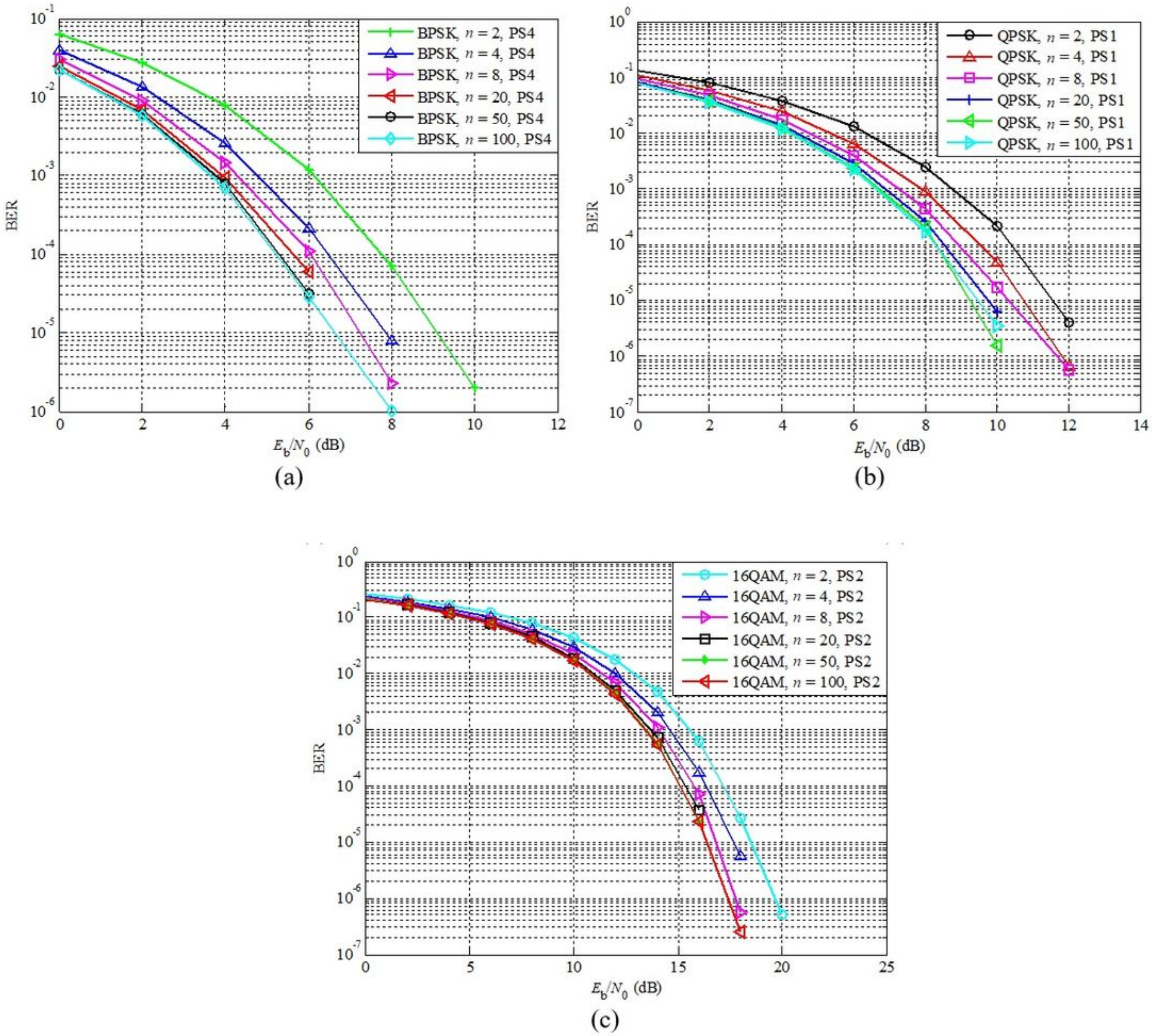

Figure 11

Fig. 11 represents the BER performance of SIMO-OFDM system under AWGN

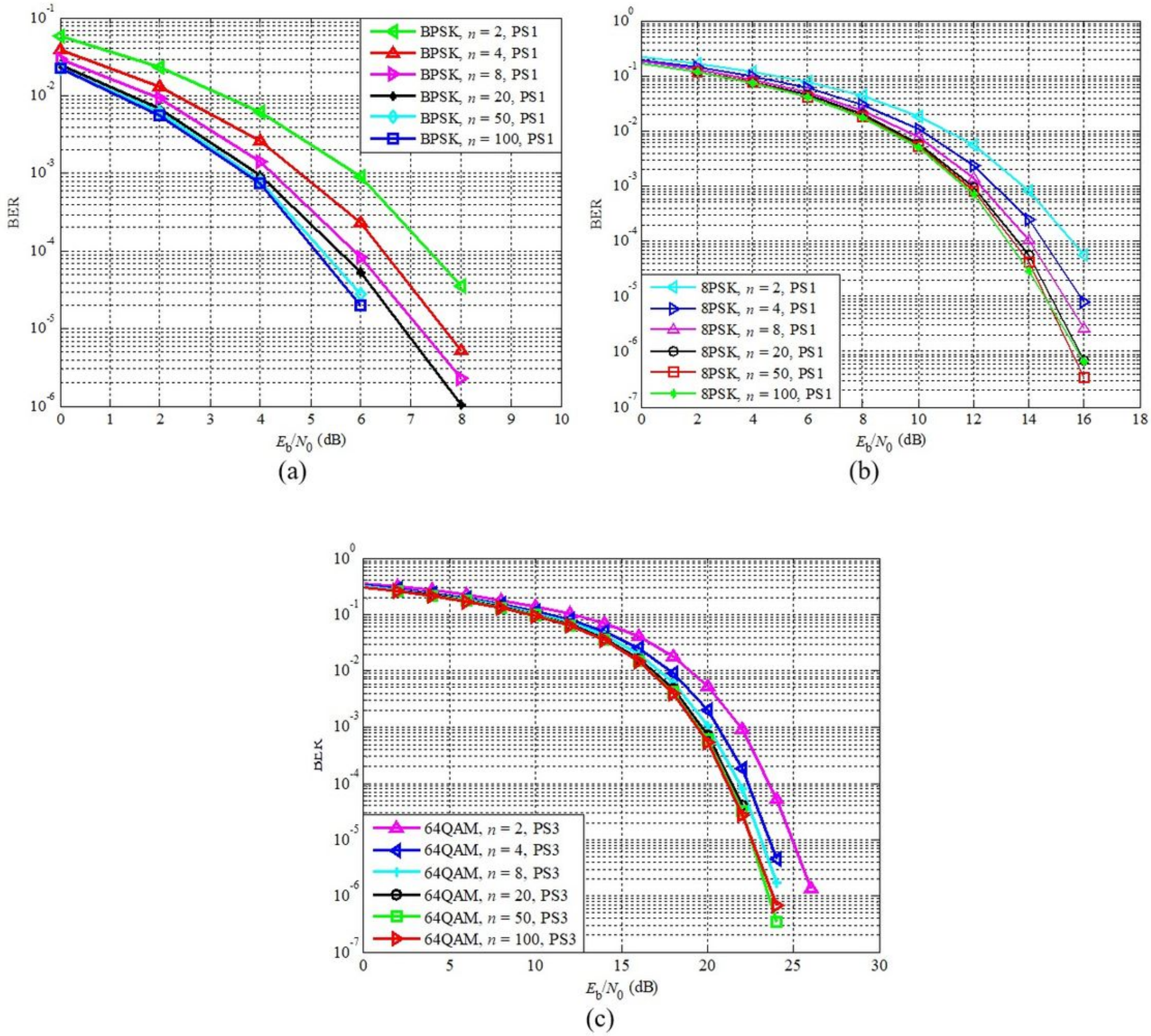

Figure 12

Fig. 12 represents the BER performance of SIMO-OFDM system under AWGN

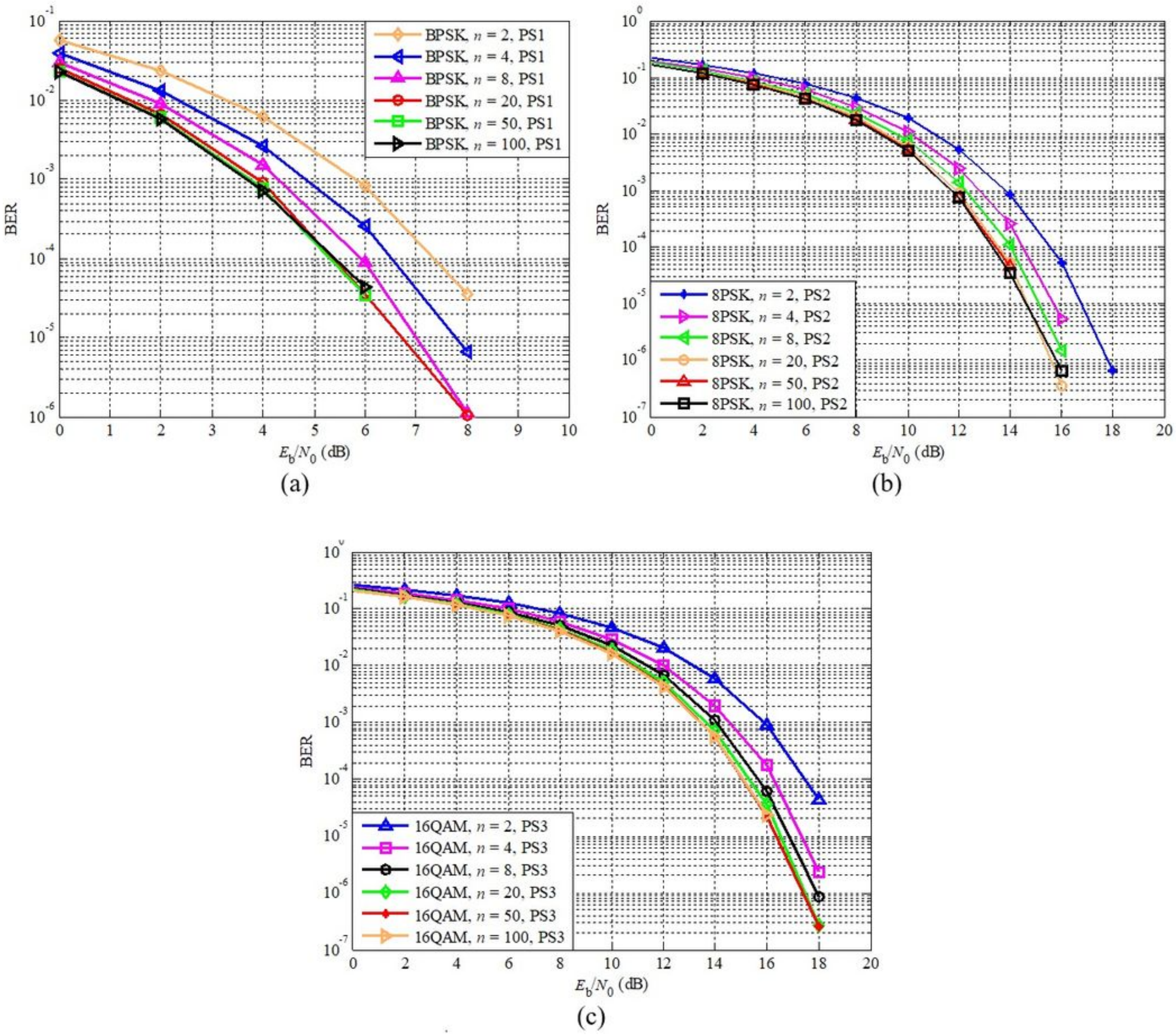

Figure 13

Fig. 13 represents the BER performance of SIMO-OFDM system under AWGN.

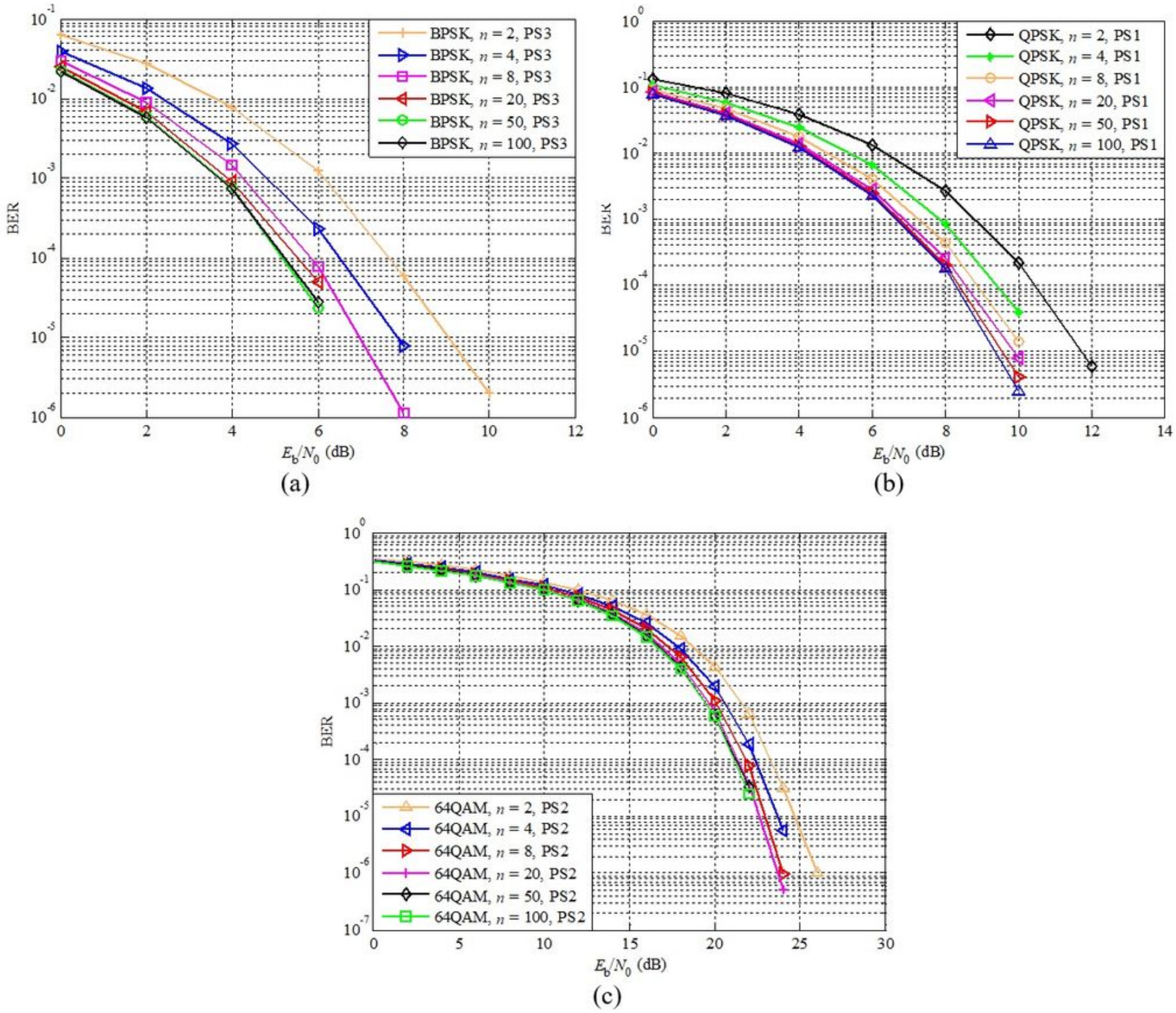

Figure 14

Fig. 14 represents the BER performance of SIMO-OFDM system under AWGN

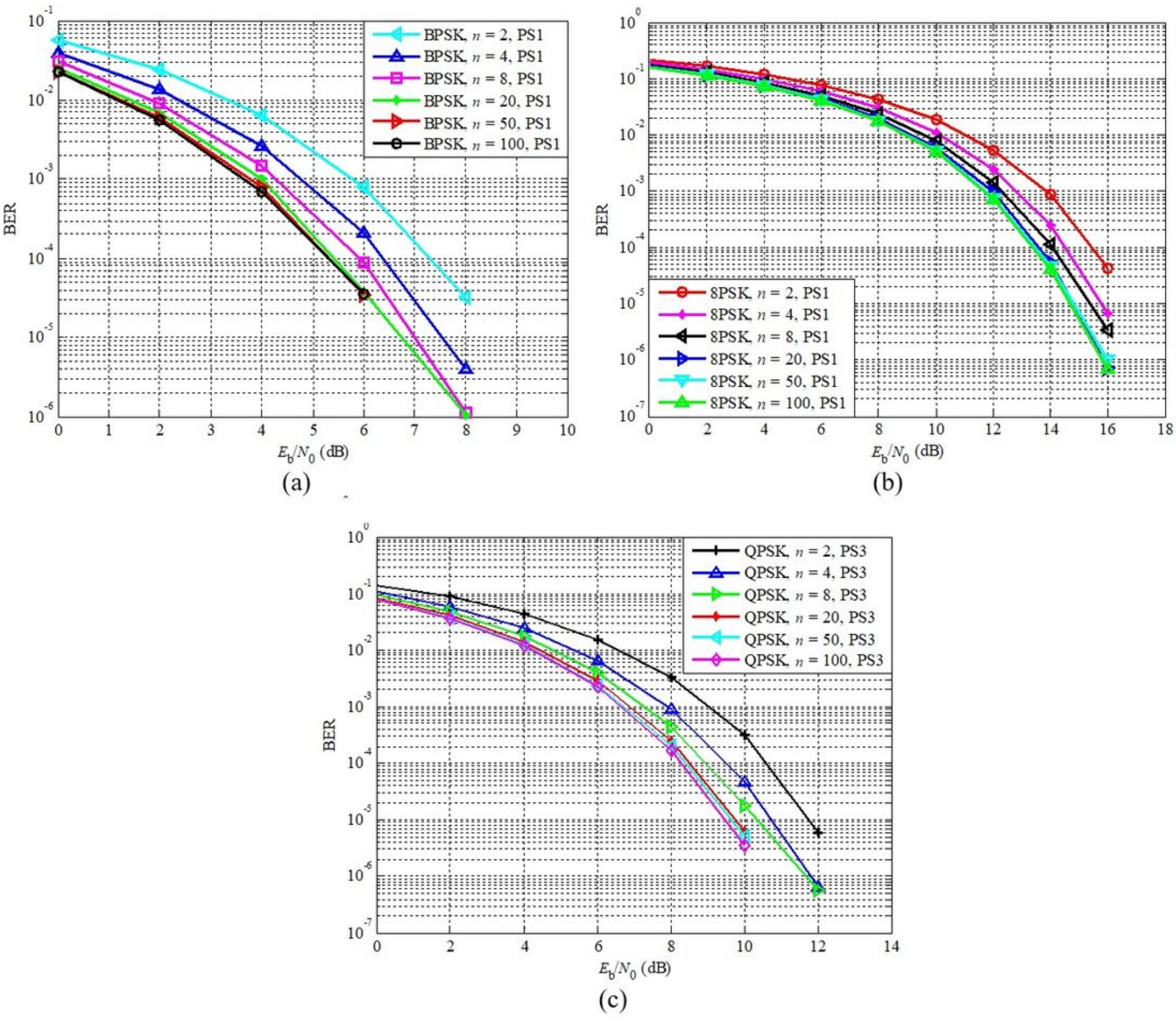

Figure 15

Fig. 15 represents the BER performance of SISO-OFDM system under AWGN.

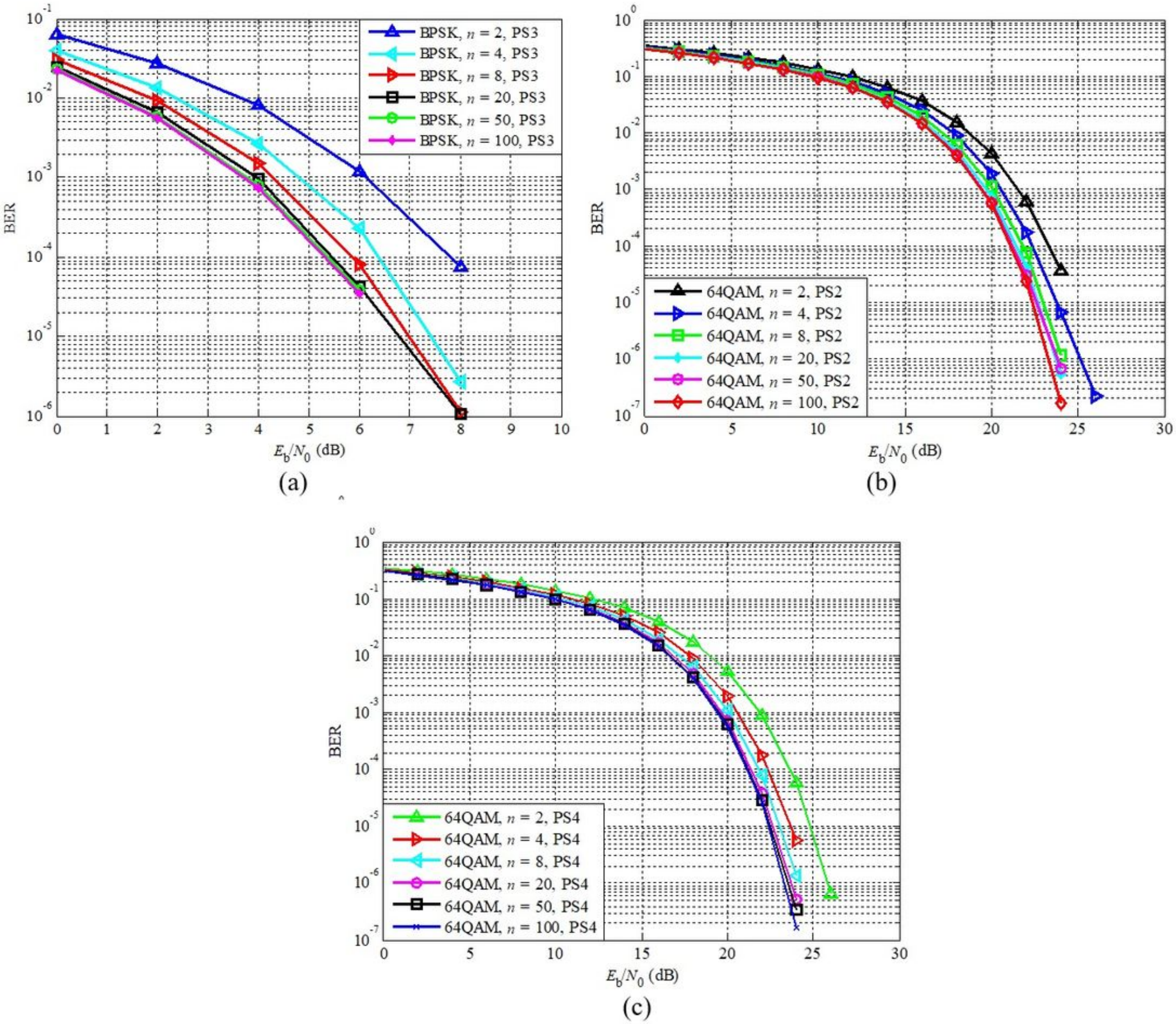

Figure 16

Fig. 16 represents the BER performance of SISO-OFDM system under AWGN

Supplementary Files

This is a list of supplementary files associated with this preprint. Click to download.

- Table1.doc